

Sound Radiation from a Perforated Plate

A. Putra

ISVR Technical Memorandum No 973

January 2007



UNIVERSITY OF SOUTHAMPTON
INSTITUTE OF SOUND AND VIBRATION RESEARCH
DYNAMICS GROUP

Sound Radiation from a Perforated Plate

by

A. Putra

ISVR Technical Memorandum No: 973

January 2007

Authorised for issue by
Professor M.J. Brennan
Group Chairman

SCIENTIFIC PUBLICATIONS BY THE ISVR

Technical Reports are published to promote timely dissemination of research results by ISVR personnel. This medium permits more detailed presentation than is usually acceptable for scientific journals. Responsibility for both the content and any opinions expressed rests entirely with the author(s).

Technical Memoranda are produced to enable the early or preliminary release of information by ISVR personnel where such release is deemed to be appropriate. Information contained in these memoranda may be incomplete, or form part of a continuing programme; this should be borne in mind when using or quoting from these documents.

Contract Reports are produced to record the results of scientific work carried out for sponsors, under contract. The ISVR treats these reports as confidential to sponsors and does not make them available for general circulation. Individual sponsors may, however, authorize subsequent release of the material.

COPYRIGHT NOTICE

(c) ISVR University of Southampton All rights reserved.

ISVR authorises you to view and download the Materials at this Web site ("Site") only for your personal, non-commercial use. This authorization is not a transfer of title in the Materials and copies of the Materials and is subject to the following restrictions: 1) you must retain, on all copies of the Materials downloaded, all copyright and other proprietary notices contained in the Materials; 2) you may not modify the Materials in any way or reproduce or publicly display, perform, or distribute or otherwise use them for any public or commercial purpose; and 3) you must not transfer the Materials to any other person unless you give them notice of, and they agree to accept, the obligations arising under these terms and conditions of use. You agree to abide by all additional restrictions displayed on the Site as it may be updated from time to time. This Site, including all Materials, is protected by worldwide copyright laws and treaty provisions. You agree to comply with all copyright laws worldwide in your use of this Site and to prevent any unauthorised copying of the Materials.

UNIVERSITY OF SOUTHAMPTON

Sound Radiation
from a Perforated Plate

Progress Report

by

Azma Putra

Faculty of Engineering, Science and Mathematics
Institute of Sound and Vibration Research

January 2007

Contents

1	Introduction	2
2	Acoustic impedance of the perforated plate	4
2.1	The effect of fluid viscosity	5
2.2	The effect of near-field	5
2.3	Condition for use of uniform acoustic impedance	9
2.4	Uniform acoustic impedance	10
3	Radiation by modes of a perforated plate in a perforated baffle	12
3.1	Wave in an infinite plate	12
3.2	Finite plate in a perforated baffle	15
3.3	Results	16
3.4	Approximate formula for IL	21
4	Radiation by modes of a perforated, unbaffled plate	23
4.1	Extended equations	23
4.2	Results	29
4.3	Approximate formula for IL at low frequency	35
5	Sound Radiation from a Baffled Plate Modelled by Discrete Sources	41
5.1	Discrete Version of Rayleigh Integral	41
5.2	Impedance matrix	43
5.3	Results	46
5.3.1	Radiation by a vibrating piston	46
5.3.2	Radiation by modes of vibration	47
5.3.3	Frequency limit of continuous impedance	50
6	Conclusions	53
A	Sound Radiation by a Uniformly Vibrating Perforated Strip	55
	References	58

Chapter 1

Introduction

The main aim in studying the sound radiated by vibrating plates is usually to determine how to reduce the sound radiation. For this purpose, several schemes have been developed including introducing perforation over the area of the plate. This technique can be seen in many practical applications, for example product collection hoppers and safety guard enclosures, such as the protective cover over flywheels and belt drives. Perforated plates are also widely used in sound absorption applications, as flexible panels covering a porous elastic material [1] or backed by an air cavity [2, 3, 4]. Besides the effect on radiated sound, it has been shown that the vibration of the perforated plate also has the effect of increasing the absorption coefficient [2].

An important parameter describing such plates is the perforation ratio. The perforation ratio is defined as the ratio of the total area of the holes to the total area of the plate S (including the holes), i.e.

$$\tau = \frac{N_o \pi r_o^2}{S} \quad (1.1)$$

where r_o is the radius of each hole (assumed circular) and N_o is the number of holes.

Several models have been proposed to calculate the sound radiation from a perforated plate. Janssens and van Vliet [5] studied the sound radiation from a vibrating steel bridge, where the effect of perforation of bridge components was investigated. Measurements were carried out on perforated plates by varying the perforation ratio, the hole density and the hole diameter. An empirical formula was then derived for the effect of perforation on the radiation efficiency.

Toyoda and Takahashi [3] proposed a model for the sound radiation from an infinite, thin elastic plate under a single normal point force excitation in the presence of a perforated plate used as an absorptive facing to the vibrating plate. The analysis was carried out under the assumption that the perforated board was rigidly attached to the vibrating

plate so that both plates have an identical motion. The problem was examined as a one-dimensional situation. In this model, the acoustic impedance of the holes was approximated by the analytical solution for wave propagation in a small tube having a circular cross section, as proposed by Maa [6]. In [4], the problem was extended to three-dimensions but still using a normal point force excitation at a particular location on the plate. A large reduction in sound radiation due to perforation on the facing was found around a narrow frequency of the Helmholtz resonator formed by the air cavity inside the honey comb structure and the perforated plate.

Fahy and Thompson [7] started with a model of radiation by plane bending waves propagating in an unbounded, uniformly perforated plate to calculate the radiation efficiency of a simply supported rectangular plate. The assumptions imply that the plate is effectively mounted in a similarly perforated rigid baffle. This model replaces the perforations by an equivalent continuous impedance.

The model was then extended to the situation where the plate and the baffle have different specific acoustic impedances. The relation between velocities and pressures was derived in the wavenumber domain as a matrix problem and then solved by matrix inversion. As a preliminary case, this was applied to the radiation by a perforated strip piston, in two dimensions, vibrating in an infinite baffle. Good results were obtained for the case of a perforated strip piston in a perforated baffle and in a rigid baffle. However, problems are found with this model at low frequencies for an un baffled perforated strip. A very low acoustic impedance of the boundary (relative to the acoustic impedance of the hole) leads to a singular or nearly singular matrix which reduces the quality of the results from the inverted matrix. In addition, expanding this model into the three-dimensional case is found to require intensive computational effort. Results from this model have been reproduced and can be seen in Appendix A.

For the case of un baffled plate, the sound radiation from a perforated plate can be calculated by modifying Laulagnet's model [8] to introduce the perforation. At low perforation ratios, it is found that the result is lower than that from the perforated baffle. However, as the perforation ratio increases, the radiation efficiency of the perforated plate in the perforated baffle and the perforated un baffled plate is found to become similar.

In Chapter 2 the impedance of the hole and its approximations in terms of fluid viscosity and near field effects are described. In Chapter 3, a model for a perforated plate in a perforated baffle is considered following [7]. In Chapter 4 the un baffled perforated plate is considered by modifying the Laulagnet's model [8]. Chapter 5 describes an alternative approach in which the perforated plate is represented by discrete monopole sources. Chapter 6 summarises the conclusions.

Chapter 2

Acoustic impedance of the perforated plate

For a circular hole in a plate of finite thickness t , its acoustic impedance (ratio between pressure and velocity) can be approximated by that of a short tube ($kt \ll 1$). The acoustic impedance of a short tube has been studied by various authors [9], [10], [11]. Maa [6] gives the following approximate formula

$$Z_h = Z_{h,R} + Z_{h,I} = \frac{p}{v_f} \quad (2.1)$$

where

$$Z_{h,R} = \frac{32\nu t}{d_o^2} \left[\left(1 + \frac{X_o^2}{32} \right)^{1/2} + \frac{\sqrt{2}}{32} X_o \frac{d_o}{t} \right]$$
$$Z_{h,I} = j\rho\omega t \left[1 + \left(9 + \frac{X_o^2}{2} \right)^{-1/2} + \left(\frac{8}{3\pi} \right) \frac{d_o}{t} \right]$$
$$X_o = \frac{d_o}{2} \sqrt{\frac{\omega\rho}{\nu}}$$

p is the sound pressure, v_f is the fluid velocity in the tube, ρ is the density of the fluid, d_o is the hole diameter and ν is the viscosity, which for air is 1.8×10^{-5} N.s/m².

The real part $Z_{h,R}$ is called the acoustic resistance and is associated with energy radiation and viscous losses. The imaginary part is termed the acoustic reactance which is inertial in nature [12]. The above formula was developed for use in the case of a micro-perforated plate (MPP) for an acoustic absorber. For effective absorption, it is suggested that the hole diameter d_o of the MPP should be between 0.05 and 1 mm and the perforation ratio τ between 0.5 and 1.5% [1], [6], [13].

2.1 The effect of fluid viscosity

The effect of the fluid viscosity ν is often taken into account in modelling microperforations. X_o is the perforation constant that includes the effect of friction between the air and the plate interface in the hole due to the viscosity.

Figure 2.1 plots the real and imaginary parts of the acoustic impedance of a 3 mm tube length for certain frequencies as a function of hole diameter. This shows that for a small hole diameter, the reactance component is almost constant. At $d_o < 0.1$ mm, the resistive component has a higher contribution to the acoustic impedance. However, the resistive component contribution decreases as the hole diameter increases. For a larger hole diameter ($d_o > 1$ mm), the contribution of the reactive component becomes more significant than that of the resistive component. Moreover, its contribution becomes more important as the frequency increases. Therefore for the purpose of the present study, where the holes are generally larger than 1 mm, it can be assumed that the fluid reaction in the holes is purely inertial (behaves like a mass). Hence the resistive component $Z_{h,R}$ will be neglected, leaving only the reactive component $Z_{h,I}$.

As ν for air is small, for larger d_o the term $()^{-1/2}$ in the reactive component is also small. It becomes much smaller than unity as the frequency increases. Hence it can be omitted from the equation and Eq.(2.1) reduces to

$$Z_h = j\rho\omega t \left[1 + \left(\frac{8}{3\pi} \right) \frac{d_o}{t} \right] \quad (2.2)$$

An end correction, i.e. $(8/3\pi)r_o$ for each end of the tube, where r_o is the hole radius, has been included here which is proportional to an added mass that corresponds to the excess kinetic energy of fluid motion due to the open end of the hole [14]. Other end corrections have also been proposed, i.e. $(\pi/4)r_o$ [9] and $0.82r_o$ [15]. However, quantitatively these values are very similar ($0.85r_o$, $0.79r_o$ and $0.82r_o$ respectively). In the remainder of this report the form $(\pi/4)r_o$ will be used as in [9].

2.2 The effect of near-field

To build a model of sound radiation from a perforated plate, one consideration is to assess the effect of the near-field from one hole on the adjacent holes. From this it should be possible to say whether the acoustic impedance of an array of holes can be derived simply from that of a single hole. The idea is to calculate the acoustic pressure on the surface of the plate as a function of distance from the centre of the hole and compare it with the acoustic pressure at the centre of the hole. If the hole is large enough to

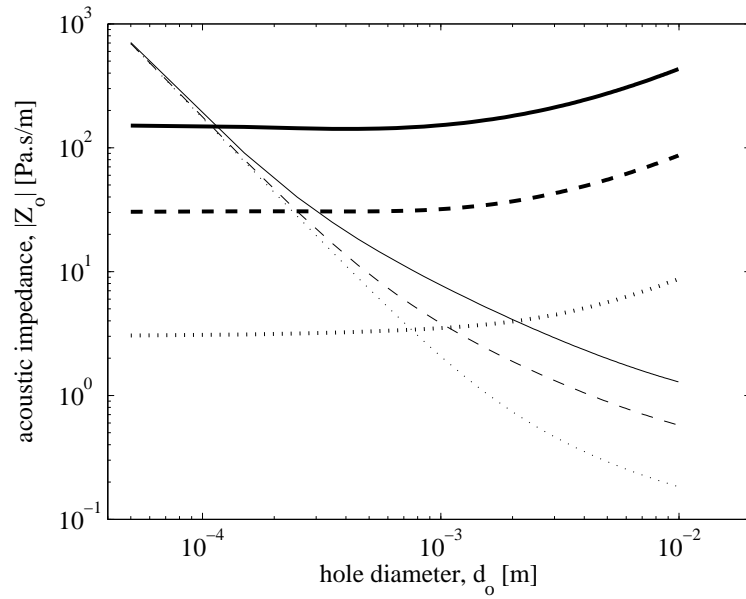


FIGURE 2.1: The magnitude of the real (thin line) and imaginary (thick line) part of the acoustic impedance of a circular hole for particular frequencies (\cdots 100, $---$ 1000 and $—$ 5000 Hz, 3 mm tube length).

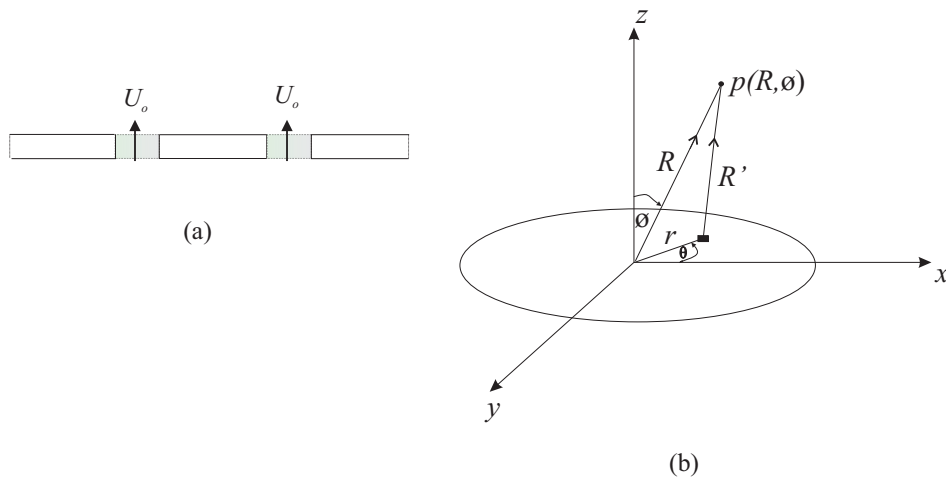


FIGURE 2.2: (a) Fluid motion inside the holes acting like a moving piston with velocity U_0 and (b) co-ordinate system of a flat piston.

ignore viscous effects at the edges, but small compared with the acoustic wavelength, the motion of fluid inside the holes can be treated as uniform across the hole area. The hole can then be represented by a piston mounted in an infinite rigid baffle, see Figure 2.2. Assuming a piston of radius r_o moves harmonically with a uniform velocity amplitude U_o , the acoustic pressure can be obtained by using the Rayleigh integral [9]

$$p(R, \phi, \theta) = \frac{jk\rho cU_o}{2\pi} \int_S \frac{e^{-jkR'}}{R'} dS \quad (2.3)$$

where R' is the distance between the point (r, θ) on the piston and the field point (R, ϕ, θ) .

Following Kinsler and Frey [16], along the z axis ($\phi = 0$), the pressure can be written as

$$p(R, \phi) \Big|_{\phi=0} = \frac{jk\rho cU_o}{2\pi} \int_0^{r_o} \frac{e^{-jk\sqrt{R^2+r^2}}}{\sqrt{R^2+r^2}} 2\pi r dr \quad (2.4)$$

The integral can be solved readily since

$$\frac{r}{\sqrt{R^2+r^2}} e^{-jk\sqrt{R^2+r^2}} = -\frac{d}{dr} \left(\frac{e^{-jk\sqrt{R^2+r^2}}}{jk} \right)$$

Then the complex acoustic pressure is

$$p(R, \phi) \Big|_{\phi=0} = \rho c U_o \left[e^{-jkR} - e^{-jk\sqrt{R^2+r_o^2}} \right] \quad (2.5)$$

The pressure at the centre p_c of the piston ($R = 0$) is then

$$p_c = p(R, \phi) \Big|_{R=0, \phi=0} = \rho c U_o \left(1 - e^{-jkr_o} \right) = \rho c U_o e^{-jkr_o/2} \left(e^{jkr_o/2} - e^{-jkr_o/2} \right) \quad (2.6)$$

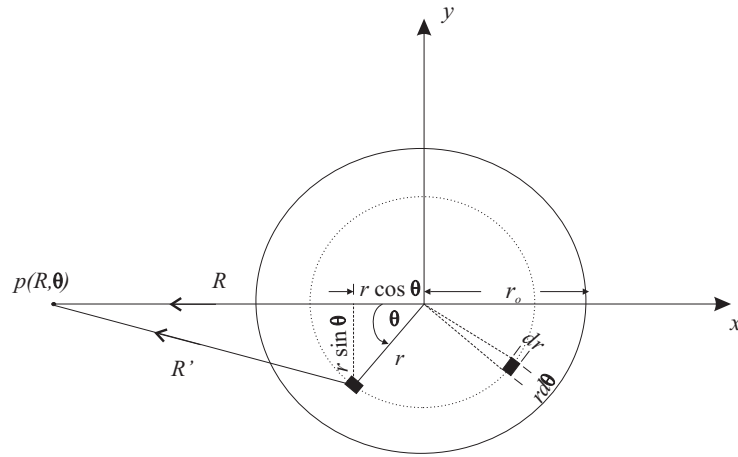
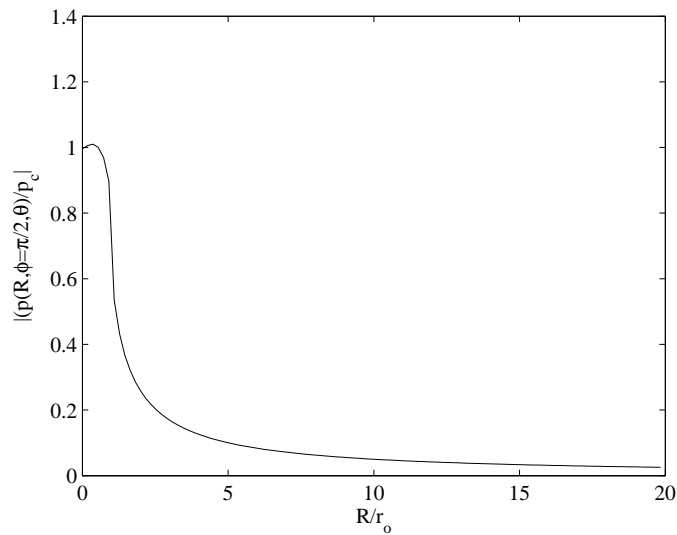
This has magnitude

$$|p_c| = 2\rho c U_o \left| \sin \left(\frac{kr_o}{2} \right) \right| \quad (2.7)$$

For a point in the plane of the piston at distance R from the centre, see Figure 2.3, the distance R' from the small element dS of the piston to the observer point can be written as

$$R' = \sqrt{(R - r \cos \theta)^2 + (r \sin \theta)^2} = \sqrt{R^2 - 2Rr \cos \theta + r^2} \quad (2.8)$$

Eq.(2.3) can now be written as

FIGURE 2.3: Co-ordinate system of a piston in xy axes plane.FIGURE 2.4: Pressure on plate surface due to a circular piston of radius r_o relative to the pressure at the centre of the piston ($kr_o \ll 1$).

$$p(R, \phi, \theta) \Big|_{\phi=\pi/2} = \frac{jk\rho cU_o}{2\pi} \int_0^{2\pi} \int_0^{r_o} \frac{e^{-jk\sqrt{R^2-2Rr\cos\theta+r^2}}}{\sqrt{R^2-2Rr\cos\theta+r^2}} r dr d\theta \quad (2.9)$$

The double integral in Eq.(2.9) is more difficult to solve analytically so a numerical calculation has been used.

Figure 2.4 plots the ratio of the acoustic pressure on the plate surface to the pressure at the centre of the piston for $kr_o \ll 1$. This is found to be independent of the frequency. The pressure falls very steeply around $R = r_o$. For values of $R > 2r_o$, the ratio becomes less than 0.25 corresponding to a sound pressure level ($\text{SPL} = 10 \log_{10} p^2$) difference of more than 12 dB which is significant. The SPL difference increases as the distance increases. Relating this to an array of holes, if $R = 2r_o$, R corresponds to the centre of

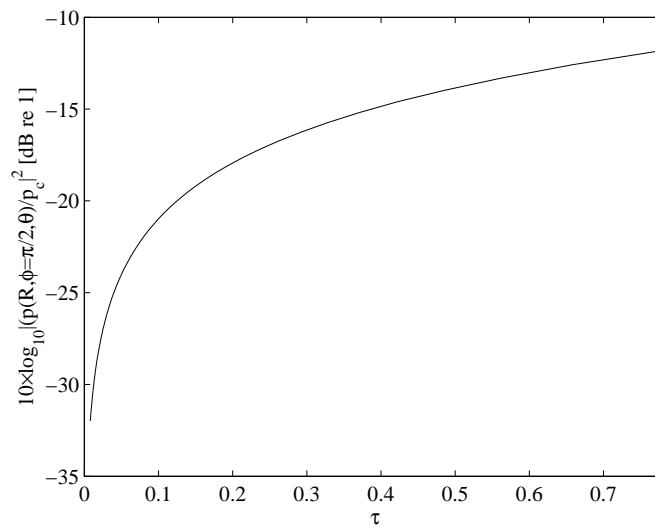


FIGURE 2.5: Pressure on plate surface due to a circular piston of radius r_o relative to the pressure at the centre of the piston plotted against the perforation ratio ($kr_o \ll 1$).

a second hole whose edge is just touching the first, which is quite an extreme form of perforation. Thus for practical situations where $R \gg 2r_o$, the pressure due to one hole can be ignored at the next. Therefore, it can be concluded that the near-field of one hole does not have a significant effect on the pressure at the adjacent holes.

Considering a perforated plate with a rectangular array of circular holes, the perforation ratio can be expressed as

$$\tau = \frac{\pi r_o^2}{R^2} \quad (2.10)$$

where R is the distance between hole centres.

Figure 2.5 presents the pressure ratio in dB scale plotted against perforation ratio. This shows that a plate can be made up to a very high perforation ratio yet still the influence of one hole on another is small. Even for the maximum perforation, the difference pressure is more than 10 dB.

2.3 Condition for use of uniform acoustic impedance

Another factor that has to be considered to have a simple model of the sound radiation from a perforated plate is the assumption that the array of holes can be replaced by a uniform layer of acoustic impedance at the surface of the plate. For this to be valid, the distance between the holes must be short enough compared with the acoustic wavelength.

Figure 2.6(a) presents the real part of the ratio between the pressure at some distance R and the pressure at the piston centre. Results are shown for different frequencies. It can

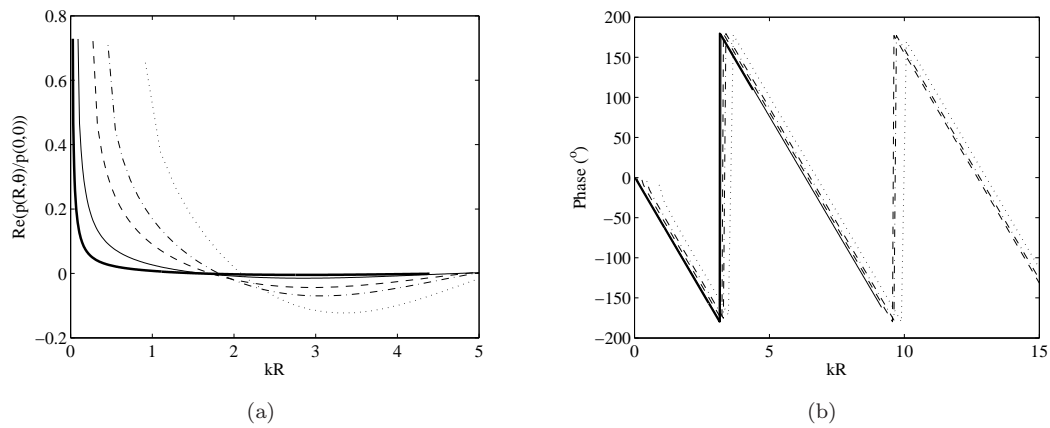


FIGURE 2.6: (a) The real part of the ratio between the pressure at a distance from and at the center of the piston and (b) the phase of the pressure ratio (— 500 Hz, - - 1 kHz, - · - 3 kHz, · · - 5 kHz, · · · 10 kHz).

be seen that the curves intersect roughly around $kR = \pi/2$. Figure 2.6(b) also shows that at $kR = \pi/2$ the phase is -90° . This suggests that the distance between holes to achieve a uniform acoustic impedance must satisfy

$$R < \frac{\pi}{2k} = \frac{\lambda}{4} \quad (2.11)$$

where λ is the acoustic wavelength. However this condition will be considered in more detail in Chapter 5.

2.4 Uniform acoustic impedance

Consider a plate with a uniform array of holes. Using Rayleigh's end correction in Eq.(2.2), the array of holes can be represented by an equivalent, continuously distributed, uniform *specific* acoustic impedance given by

$$z_h = \frac{Z_h}{\tau} = \frac{j\rho\omega t}{\tau} \left[1 + \left(\frac{\pi}{4} \right) \frac{d_o}{t} \right] \quad (2.12)$$

where τ is the perforation ratio.

Using $k = \omega/c$, this can be expressed as

$$z_h = j\rho c \left[\frac{kt}{\tau} \left(1 + \frac{\pi d_o}{4t} \right) \right] = j\rho c h \quad (2.13)$$

where h is the non-dimensional specific acoustic reactance, which can be written as

$$h = \frac{k}{\tau} \left(t + \frac{\pi d_o}{4} \right) \quad (2.14)$$

In Chapter 5, the plate and the holes are modelled with discrete sources, i.e. an array of monopole sources that contribute to the sound radiation. This allows the frequency limit of the uniform acoustic impedance to be verified in terms of distance between holes.

Chapter 3

Radiation by modes of a perforated plate in a perforated baffle

3.1 Wave in an infinite plate

For a plane, harmonic, bending wave of frequency ω and wavenumber k_x propagating in the x -direction in an infinite plate, the specific acoustic impedance presented to the upper surface of the plate by the fluid, $z_a(k_x)$, is given by [12]

$$z_a(k_x) = \frac{\tilde{P}(k_x)}{\tilde{V}(k_x)} = \frac{\omega\rho}{(k^2 - k_x^2)^{1/2}}, \quad k_x < k \quad (3.1)$$

where $\tilde{P}(k_x)$ and $\tilde{V}(k_x)$ are the complex acoustic pressure and the plate velocity amplitude respectively. For $k_x > k$, $z_a(k_x)$ is imaginary (reactive). Only the real part of $z_a(k_x)$ is required here to calculate the propagating waves producing sound radiation. The imaginary part produces a near field.

In the case of a perforated plate, as shown in Figure 3.1, following the method of [7] the difference between the local pressures on the upper and lower surfaces of the plate drives fluid through the individual holes. In turn, these pressures are modified by the flow through the holes. Considering the holes as a continuous distribution, an equivalent fluid particle velocity $v_f(x)$, due to the flow through the holes relative to the plate, can be given by

$$v_f(x) = -2\frac{p_a(x)}{z_h} \quad (3.2)$$

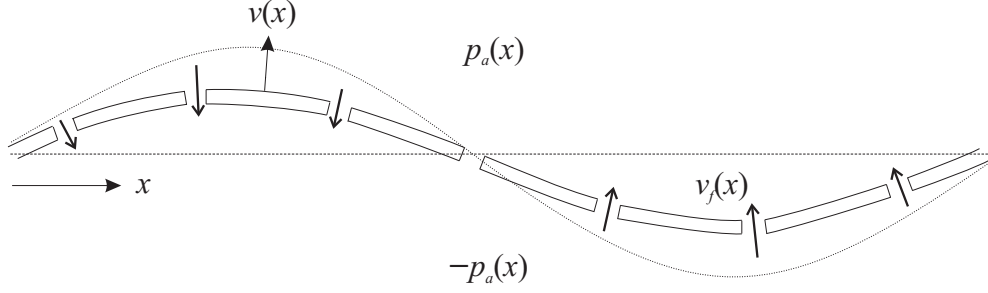


FIGURE 3.1: Analytical model of a perforated plate

where p_a is the upper surface pressure resulting from the combination of the plate $v(x)$ velocity and equivalent continuously distributed fluid velocity through the holes $v_f(x)$ (the pressure on the lower surface is $-p_a$) and z_h is given by Eq.(2.13). Therefore for the perforated plate, the net velocity formed of the combination of the normal velocity of plate and the continuously distributed fluid motion v_p is given by

$$v_p(x) = v(x) + v_f(x) = v(x) - 2\frac{p_a(x)}{z_h} \quad (3.3)$$

Since the plate is infinite and the bending wave has a unique wavenumber k_x , the plate and the equivalent fluid particle velocity also have the same unique wavenumber in the x direction. Eq.(3.3) can be expressed as

$$\tilde{V}_p(k_x) = \tilde{V}(k_x) + \tilde{V}_f(k_x) = \tilde{V}(k_x) - 2\frac{\tilde{P}_a(k_x)}{z_h} \quad (3.4)$$

From Eq.(3.1), this generates the pressure \tilde{P}_a

$$\tilde{P}_a(k_x) = \tilde{V}_p(k_x)z_a(k_x) = \left(\tilde{V}(k_x) - 2\frac{\tilde{P}_a(k_x)}{z_h} \right) z_a(k_x) \quad (3.5)$$

Rearranging yields

$$\tilde{P}_a(k_x) = \frac{z_h z_a(k_x)}{z_h + 2z_a(k_x)} \tilde{V}(k_x) \quad (3.6)$$

Substituting the Fourier transform of Eq.(3.2) into Eq.(3.6)

$$\tilde{V}_f(k_x) = \frac{-2z_a(k_x)}{z_h + 2z_a(k_x)} \tilde{V}(k_x) \quad (3.7)$$

Finally substituting Eq.(3.6) into Eq.(3.4) yields the ratio of the complex amplitudes of the total normal velocity of plate and fluid flow through the holes to that of the plate

$$\frac{\tilde{V}_p(k_x)}{\tilde{V}(k_x)} = \frac{1}{1 + 2z_a(k_x)/z_h} \quad (3.8)$$

Eq.(3.8) confirms that the sound radiation from the plate is reduced by introducing perforation to the plate. As $|z_a(k_x)/z_h| \rightarrow \infty$, i.e. open area condition (absence of the plate), the ratio tends to zero so that flow through the holes completely compensates the plate motion, while as $z_a(k_x)/z_h \rightarrow 0$, i.e. the unperforated plate (absence of the holes), the ratio tends to unity.

The sound power radiated per unit area of the perforated plate can be calculated by

$$W_p(k_x) = \frac{1}{2} \Re \left\{ \tilde{P}(k_x) \tilde{V}_p^*(k_x) \right\} \quad (3.9)$$

By using the relation from Eq.(3.1)

$$W_p(k_x) = \frac{1}{2} \Re \left\{ z_a(k_x) \tilde{V}_p(k_x) \tilde{V}_p^*(k_x) \right\} = \frac{1}{2} \left| \tilde{V}_p(k_x) \right|^2 \Re \{ z_a(k_x) \} \quad (3.10)$$

The ratio of sound power per unit area of the perforated plate to that of the unperforated plate is therefore given by

$$\frac{W_p(k_x)}{W(k_x)} = \left| \frac{\tilde{V}_p(k_x)}{\tilde{V}(k_x)} \right|^2 = \frac{1}{1 + 4(z_a(k_x)/|z_h|)^2}, \quad k_x < k \quad (3.11)$$

since z_h is imaginary.

In terms of the non-dimensional specific acoustic reactance h , the ratio $z_a(k_x)/|z_h|$ can be expressed as

$$\frac{z_a(k_x)}{|z_h|} = \frac{1}{h(1 - k_x^2/k^2)^{1/2}} = \frac{1}{h(1 - \alpha^2)^{1/2}}, \quad \alpha < 1 \quad (3.12)$$

where $\alpha = k_x/k$.

For a plane wave travelling with components in the x and y directions, k_x^2 is replaced by the square of the resultant $k_x^2 + k_y^2$. It follows that Eq.(3.12) can be written as

$$\frac{z_a(k_x, k_y)}{|z_h|} = \frac{1}{h(1 - \alpha^2 - \beta^2)^{1/2}}, \quad \alpha^2 + \beta^2 < 1 \quad (3.13)$$

where $\beta = k_y/k$.

3.2 Finite plate in a perforated baffle

From the infinite plate case, the situation can be extended to the case of modes of vibration in a finite plate which can be decomposed into a spectrum of travelling waves.

Consider a rectangular plate set in an infinite baffle. For convenience at this stage, the baffle is assumed to be similarly perforated to the plate so that the previous analysis can be used. Suppose the plate is vibrating in mode (m, n) . The plate vibration can be defined by its non-dimensional wavenumber spectrum over (α, β) . From Eq.(3.11), the ratio of the squared amplitudes of the total normal velocity of plate and fluid flow through the holes to that of the unperforated plate velocity, for the mode (m, n) at non-dimensional wavenumber (α, β) is given by

$$|X(\alpha, \beta)|^2 = \left| \frac{\tilde{V}_{p,mn}(\alpha, \beta)}{\tilde{V}_{mn}(\alpha, \beta)} \right|^2 = \frac{h^2(1 - \alpha^2 - \beta^2)}{4 + h^2(1 - \alpha^2 - \beta^2)}, \quad \alpha^2 + \beta^2 < 1 \quad (3.14)$$

Recalling Eq.(3.10) for two-dimensional, the total sound power over the infinite range of wavenumbers can be written as

$$\overline{W} = \frac{1}{8\pi^2} \Re \int_{-\infty}^{\infty} \int_{-\infty}^{\infty} \frac{\omega \rho}{(k^2 - k_x^2 - k_y^2)^{1/2}} |\tilde{V}(k_x, k_y)|^2 dk_x dk_y \quad (3.15)$$

Only wavenumber components satisfying the condition $(k_x^2 + k_y^2)^{1/2} \leq k$ contribute to sound power radiation; elsewhere the term $(k^2 - k_x^2 - k_y^2)^{1/2}$ is imaginary. The range of integration can therefore be limited to give

$$\overline{W} = \frac{\rho c}{8\pi^2} \int_{-k}^k \int_{-\sqrt{k^2 - k_x^2}}^{\sqrt{k^2 - k_x^2}} \frac{k}{(k^2 - k_x^2 - k_y^2)^{1/2}} |\tilde{V}(k_x, k_y)|^2 dk_x dk_y \quad (3.16)$$

In the two-dimensional spatial Fourier transform, the velocity distribution of an individual mode is decomposed into a continuous spectrum of spatially harmonic, travelling plane wave components, each having a certain wavenumber vector (k_x, k_y) :

$$\tilde{V}_{mn}(k_x, k_y) = \int_0^a \int_0^b u_{mn} \varphi_{mn} e^{-j(k_x x + k_y y)} dx dy \quad (3.17)$$

where $\tilde{V}_{mn}(k_x, k_y)$ is the complex amplitude of the wavenumber component. Integration yields [12]

$$\tilde{V}(\alpha, \beta) = u_{mn} \Lambda k^{-2} (\varepsilon + j\vartheta)(\gamma + j\varsigma) \quad (3.18)$$

where

$$\Lambda = \frac{\left(\frac{m\pi}{ka}\right) \left(\frac{n\pi}{kb}\right)}{\left[\alpha^2 - \left(\frac{m\pi}{ka}\right)^2\right] \left[\beta^2 - \left(\frac{n\pi}{kb}\right)^2\right]}$$

$$\varepsilon = (-1)^m \cos(\alpha ka) - 1, \quad \vartheta = (-1)^{m+1} \sin(\alpha ka)$$

$$\gamma = (-1)^n \cos(\beta kb) - 1, \quad \varsigma = (-1)^{n+1} \sin(\beta kb)$$

in which $\alpha = k_x/k$ and $\beta = k_y/k$ are the non-dimensional wavenumbers and a and b are the plate dimensions.

Substituting Eq.(3.18) into Eq.(3.16), the sound power radiated by a single mode is thus

$$\overline{W}_{mn} = \frac{\rho c \overline{|u_{mn}|^2}}{8\pi^2 k^2} \int_{-1}^1 \int_{-\sqrt{1-\alpha^2}}^{\sqrt{1-\alpha^2}} \Lambda^2 \frac{(\Gamma^2 + \Pi^2)}{(1 - \alpha^2 - \beta^2)^{1/2}} d\beta d\alpha \quad (3.19)$$

where $\Gamma = (\varepsilon\gamma - \vartheta\varsigma)$ and $\Pi = (\vartheta\gamma + \varepsilon\varsigma)$. Because only spectral components of \tilde{V}_{mn} with $\alpha^2 + \beta^2 \leq 1$ can radiate sound to the far field, the integrals over α and β are calculated for the area of non-dimensional wavenumber space enclosed by a circle of unit radius centred on the origin.

Therefore to calculate the sound power radiated by a mode of a perforated plate, $|X(\alpha, \beta)|^2$ from Eq.(3.14) can be inserted into Eq.(3.19). This equation now becomes

$$\overline{W}_{p,mn} = \frac{\rho c \overline{|u_{mn}|^2}}{8\pi^2 k^2} \int_{-1}^1 \int_{-\sqrt{1-\alpha^2}}^{\sqrt{1-\alpha^2}} |X(\alpha, \beta)|^2 \Lambda^2 \frac{(\Gamma^2 + \Pi^2)}{(1 - \alpha^2 - \beta^2)^{1/2}} d\beta d\alpha \quad (3.20)$$

The radiation efficiency for a mode (m, n) of the perforated plate set in the infinite perforated baffle is then given by

$$\sigma_{mn} = \frac{1}{\pi^2 (ka)(kb)} \int_{-1}^1 \int_{-\sqrt{1-\alpha^2}}^{\sqrt{1-\alpha^2}} |X(\alpha, \beta)|^2 \Lambda^2 \frac{(\Gamma^2 + \Pi^2)}{(1 - \alpha^2 - \beta^2)^{1/2}} d\beta d\alpha \quad (3.21)$$

The total sound radiation can be calculated by modal summation in the same way as for the unperforated plate [17].

3.3 Results

With the same plate dimensions and properties as in the previous review report [18], Figure 3.2 shows the results of the modal and average radiation efficiencies of a plate having 5% perforation ratio with 5 mm diameter holes. As seen from the figure, at very

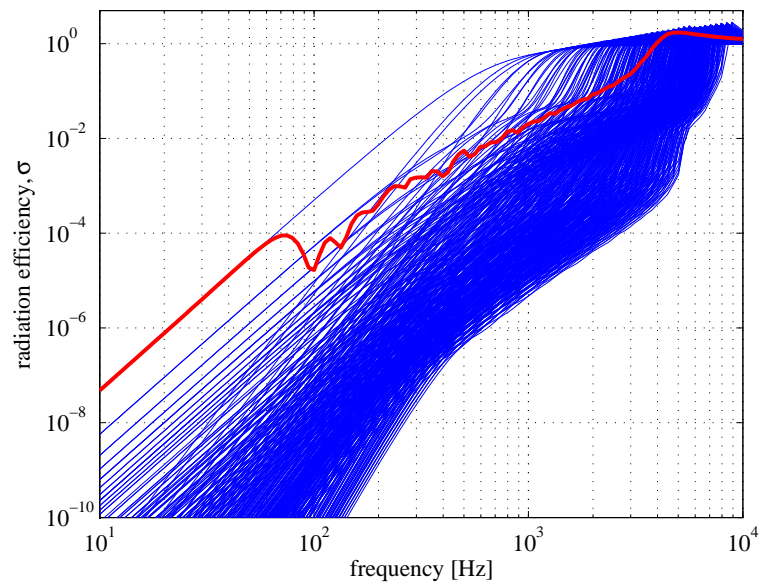


FIGURE 3.2: Modal and average radiation efficiency of a simply supported rectangular perforated plate in an infinite perforated baffle ($0.65 \times 0.5 \times 0.003$ m aluminium plate with $\eta = 0.1$; $d_o = 5$ mm, $\tau = 5\%$):—, modal radiation efficiency; —, average radiation efficiency.

low frequencies (at and below the fundamental mode at 70 Hz), instead of increasing at 20 dB/decade as the unperforated plate does, the average radiation efficiency of the perforated plate now increases at 40 dB/decade, where the additional 20 dB/decade is due to the effect of the holes. The motion of the fluid in the holes is in the opposite direction to that of the plate, i.e. 180° out of phase. The field produced by the surface sources of the plate in the vicinity of the holes is largely suppressed by the opposite fluid motion through the holes. Hence below the natural frequency of the fundamental mode, the motion of the plate and the fluid in the holes can be associated with the motion of two monopole sources acting in opposite directions which now constitute a dipole source. In the ‘corner mode’ region, from 100 to 1000 Hz, the average radiation efficiency has a frequency dependence of about 20 dB/decade, whereas for the unbaffled plate it is approximately independent of frequency.

Figure 3.3 plots the average radiation efficiencies obtained with various perforation ratios τ and constant hole diameter d_o and also the radiation efficiency of the unperforated plate for comparison. It can be seen that as the perforation ratio increases the radiation efficiency is simply reduced by an amount that is approximately constant over the frequency range.

In order to show the effect of the perforation on the sound radiation, the results are presented as the sound radiation of a perforated plate relative to that of the equivalent unperforated plate. The terminology of insertion loss can be used for this purpose. The

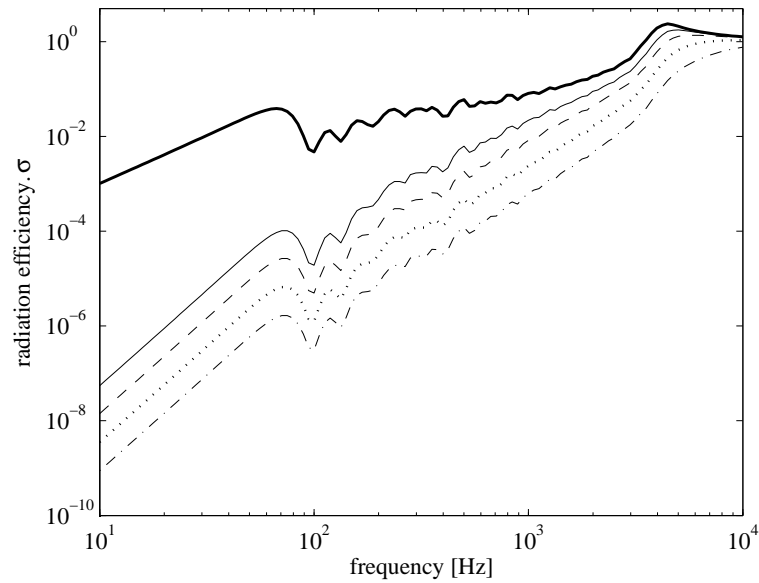


FIGURE 3.3: Average radiation efficiency of a simply supported rectangular perforated plate in an infinite perforated baffle ($0.65 \times 0.5 \times 0.003$ m aluminium plate with $\eta = 0.1$; $d_o=5$ mm: — unperforated, $\tau=$ - 5%, -- 10%, \cdots 20% and - . - 40%).

insertion loss (IL) of the perforation is defined as

$$IL = -10 \log_{10} \left(\frac{W_p}{W} \right) \quad (3.22)$$

where W_p and W are the overall radiated power of the perforated and the unperforated plate respectively. The $-IL$ gives the effect of perforation which will be used throughout the rest of this report to present the results.

Figure 3.4 plots the effect of perforation ($-IL$). Figure 3.5 show results with a constant perforation ratio and various hole diameters which shows that the sound radiation can be further reduced by reducing the hole diameter, i.e. increasing the number of holes per unit area of the plate (hole density). From Eq.(2.14), for a thin plate where the plate thickness is much smaller than the hole radius, $t \ll d_o$, the non-dimensional specific acoustic reactance can be expressed as $h = k\pi d_o / (4\tau)$. Consequently, the effect of perforation is controlled by a factor of d_o/τ . As seen from Figure 3.4 and Figure 3.5, with the same values of d_o/τ , the effect of the perforation is almost equal. For example $d_o = 10$ mm, $\tau = 10\%$ and $d_o = 20$ mm, $\tau = 20\%$ give very similar results.

Figure 3.6 presents the results for different thicknesses and dimensions of the plate. Figure 3.6(c) and Figure 3.6(d) clearly show that for this model, the effect of perforation does not depend on the plate dimensions. Compare also with Figure 3.4. The effect of

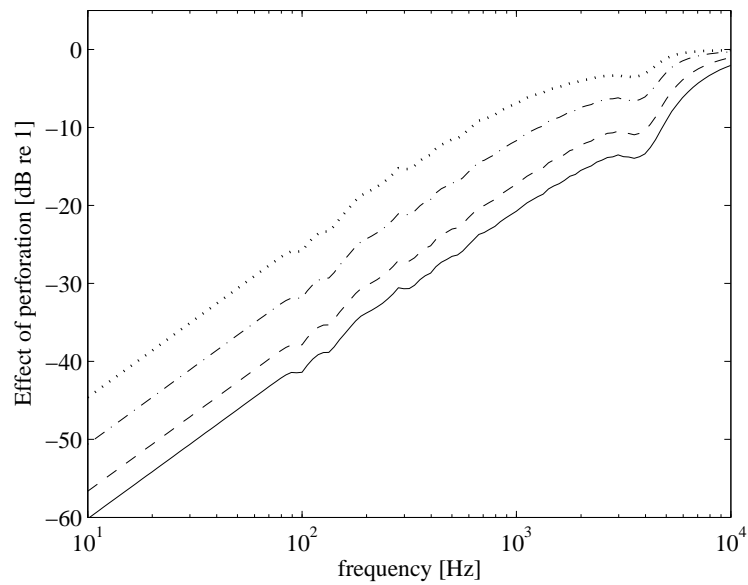


FIGURE 3.4: Effect of perforation on sound power radiation of a simply supported rectangular perforated plate in an infinite perforated baffle ($0.65 \times 0.5 \times 0.003$ m aluminium plate with $\eta = 0.1$, $d_o = 10$ mm; $\cdots \tau = 10\%$, $- \cdot - \tau = 20\%$, $-- \tau = 40\%$ mm, $- \tau = 60\%$).

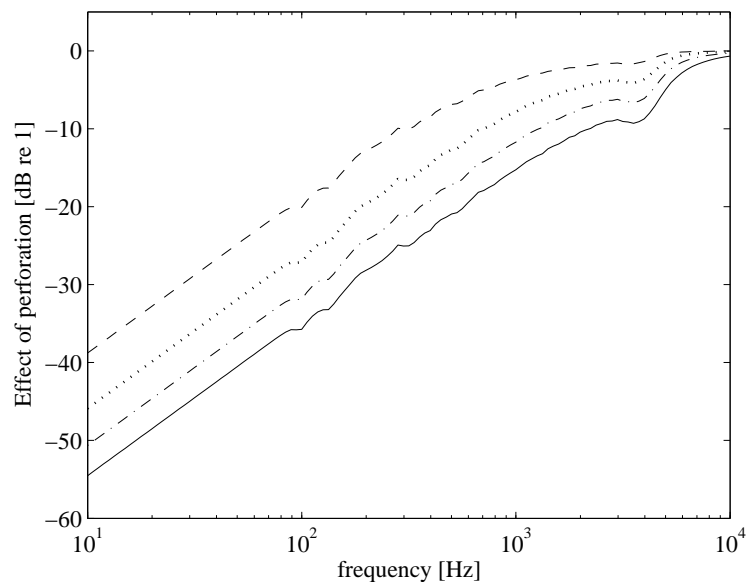


FIGURE 3.5: Effect of perforation on sound power radiation of a simply supported rectangular perforated plate in an infinite perforated baffle ($0.65 \times 0.5 \times 0.003$ m aluminium plate with $\eta = 0.1$, $\tau = 20\%$; $- d_o = 5$ mm, $- \cdot - d_o = 10$ mm, $\cdots d_o = 20$ mm, $-- d_o = 50$ mm).

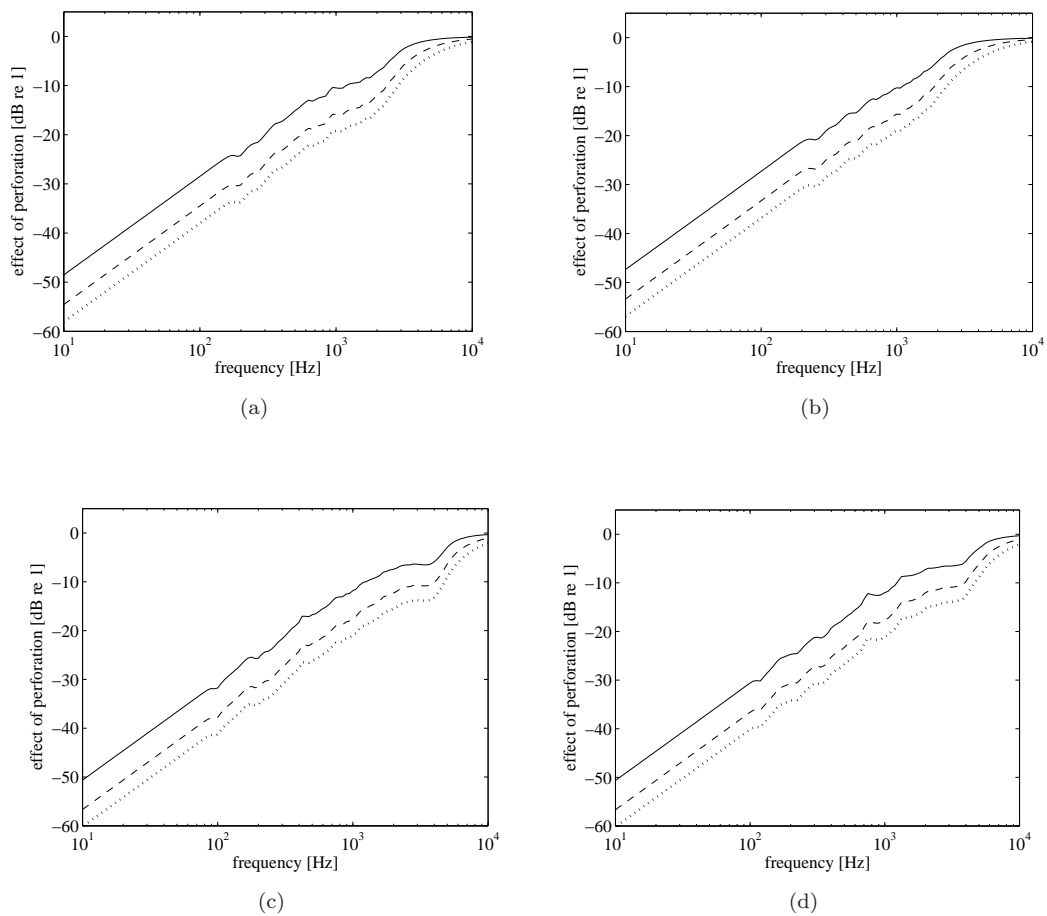


FIGURE 3.6: Effect of perforation on sound power radiation of a simply supported rectangular perforated plate in a perforated baffle for different thicknesses; (a) $0.65 \times 0.5 \times 0.006$ m, (b) $0.65 \times 0.5 \times 0.008$ m and dimensions; (c) $0.75 \times 0.4 \times 0.003$ m, (d) $0.9 \times 0.3 \times 0.003$ m (aluminium plate with $\eta = 0.1$; $d_o = 10$ mm, $\tau =$ — 20%, -- 40%, \cdots 60%).

perforation is affected only by the perforation ratio, the plate thickness and the hole size (see Eq.(2.14)).

The results can also be plotted against the non-dimensional acoustic reactance h . It can be seen from Figure 3.7 that for different dimensions and thicknesses, all the results collapse to a single line apart from small differences among the results that occur close to the critical frequency. Because the effect of perforation is independent of the plate dimensions, the curves are identical for similar plate thickness (see blue and black curves).

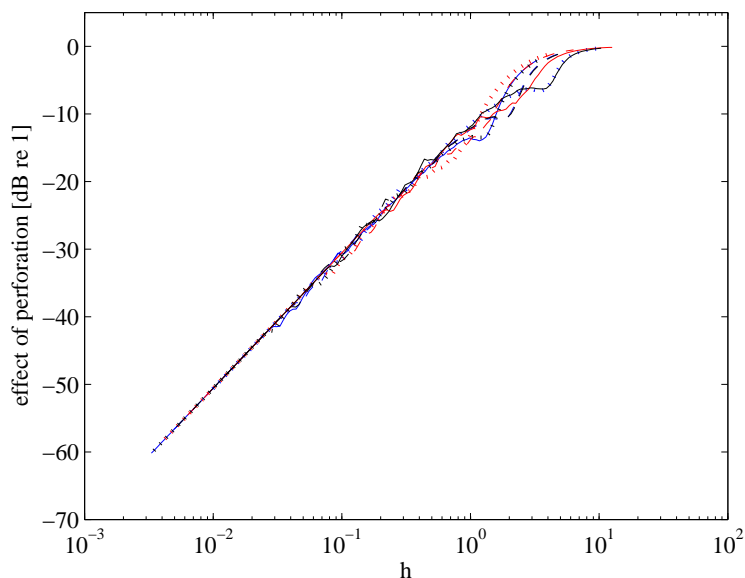


FIGURE 3.7: Effect of perforation on sound power radiation of a simply supported rectangular perforated plate in an infinite perforated baffle plotted against h ($0.65 \times 0.5 \times 0.003$ m (blue line), $0.65 \times 0.5 \times 0.006$ m (red line) and $0.75 \times 0.4 \times 0.003$ m (black line); aluminium plate with $\eta = 0.1$, $d_o = 10$ mm; $\tau =$ — 20%, -- 40%, \cdots 60%).

3.4 Approximate formula for IL

The differences in the effect of perforation at high frequencies are due to the results around and above the critical frequency as each curve converges to 0 dB. Neglecting this, an approximation can be made, at least up to the corner mode region of the sound radiation. The formula can be written as

$$-IL_{approx} = 20 \log_{10}(h) - 10.77, \quad h < h_c/2 \quad (3.23)$$

where h_c is the non-dimensional acoustic reactance at the critical frequency, f_c . Figure 3.8 plots the results comparing the analytical ($-IL$) and approximated ($-IL_{approx}$) effect of perforation. It shows good agreement between the results until $h_c/2$.

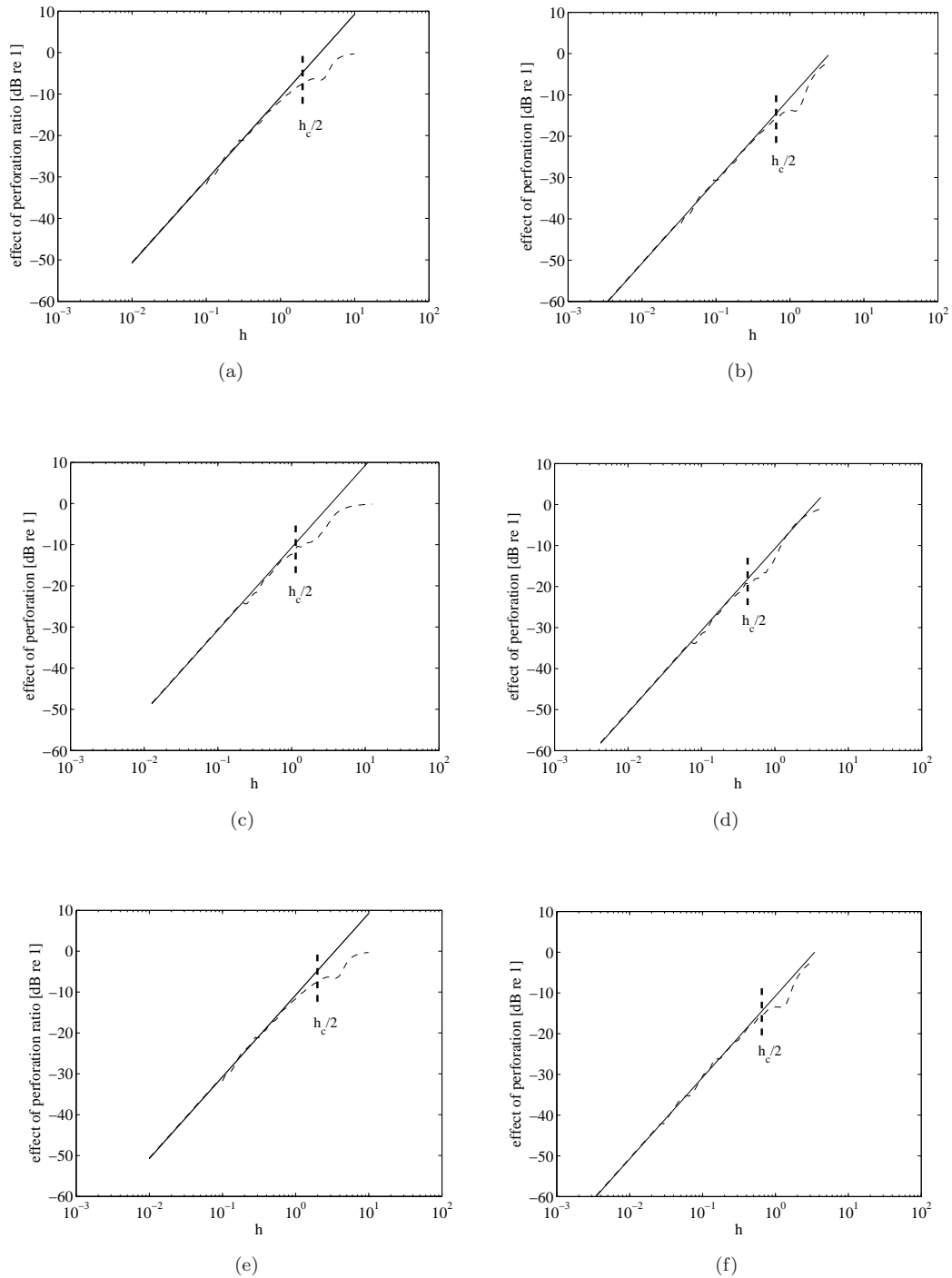


FIGURE 3.8: Comparison of exact (—) and approximated (---) effect of perforation ($-IL$) of a simply supported plate in an infinite perforated baffle. (a) and (b) $0.65 \times 0.5 \times 0.003$ m, (c) and (d) $0.65 \times 0.5 \times 0.006$ m, (e) and (f) $0.75 \times 0.4 \times 0.003$ m; (a), (c), (e): $\tau=20\%$ and (b), (d), (f): $\tau=60\%$ (aluminium plate with $\eta = 0.1$; $d_o=10$ mm).

Chapter 4

Radiation by modes of a perforated, unbaffled plate

Although mathematically convenient, a perforated plate set in a similarly perforated baffle is not an important issue, as such a situation is rarely found in practice. The more interesting case is where the baffle has a different acoustic impedance, such as the perforated plate mounted in a rigid baffle or the unbaffled perforated plate. The latter especially is frequently found in real applications and is discussed in this section.

4.1 Extended equations

The method of Laulagnet [8] for the sound radiation of an unbaffled plate discussed in the previous review [18] can be extended to introduce perforation on the plate. The flexural wave equation of a plate excited by a point force can be written as

$$B\nabla^4 w(x, y) - m\omega^2 w(x, y) = F(x, y) + \Delta p(x, y) \quad (4.1)$$

From Figure 4.1, following Laulagnet [8], the two-unknown fields, i.e. the acoustic field $p(M)$ and the vibration of the plate $w(Q)$ can be related using Euler's function in the plane of the plate at $z=0$.

$$\begin{aligned} \frac{\partial p}{\partial z}(M)|_{z=0} &= \rho \omega^2 w(M) \\ &= \int_{S_p} [B\nabla^4 w(Q) - m\omega^2 w(Q) - F(Q)] \frac{\partial^2 G(Q, M)}{\partial z_Q \partial z_M} dS_p \end{aligned} \quad (4.2)$$

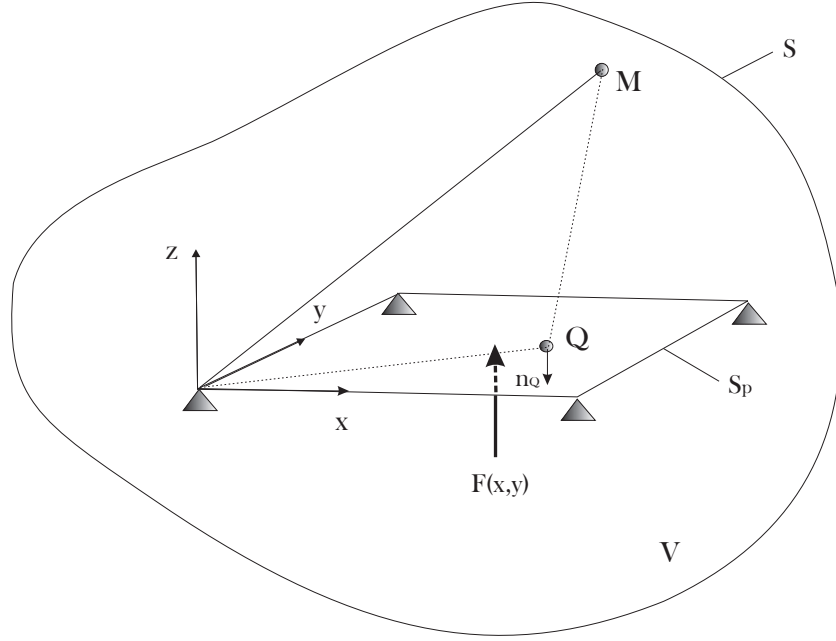


FIGURE 4.1: A simply supported plate enclosed by a volume V in the medium with its bounding surface S .

The motion of the fluid inside the holes depends on the pressure difference $\Delta p(x, y)$ between the two sides of the plate surface. The specific acoustic impedance of the distribution of holes can then be expressed as

$$z_h = \frac{\Delta p(x, y)}{v_f(x, y)} \quad (4.3)$$

where $v_f(x, y)$ is the velocity of the fluid in the holes.

With the coordinate system of the plate as in Figure 4.1, by using Euler's function on the plate surface at $z = 0$ and substituting Eq. (4.3), the relation can be written as

$$\begin{aligned} \frac{\partial p}{\partial z}(M)|_{z=0} &= \rho \omega^2 (w(M) - w_f(M)) = \rho \omega^2 w(M) + j\rho \omega v_f(M) \\ &= \rho \omega^2 w(M) + \frac{j\rho \omega}{z_h} \Delta p(M) \end{aligned} \quad (4.4)$$

where M is a point in the medium above the plate, w_f is the fluid displacement relative to the plane $z = 0$ and where $v_f = j\omega w_f$.

Substituting from Eq.(4.1) gives

$$\frac{\partial p}{\partial z}(M)|_{z=0} = \rho \omega^2 w(M) + \frac{j\rho \omega}{z_h} (B\nabla^4 w(M) - m\omega^2 w(M) - F(M)) \quad (4.5)$$

Recalling Eq.(4.2) and substituting Eq.(4.5) yields

$$\begin{aligned} \rho \omega^2 w(M) + \frac{j\rho\omega}{z_h} (B\nabla^4 w(M) - m\omega^2 w(M) - F(M)) \\ = \int_{S_p} (B\nabla^4 w(Q) - m\omega^2 w(Q) - F(Q)) \frac{\partial^2 G(Q, M)}{\partial z_Q \partial z_M} dS_p \end{aligned} \quad (4.6)$$

where Q is a point on the plate surface and the second term on the left-hand side has been added by the perforation.

The displacement can be considered as the summation of a series of plate modes,

$$w(x, y) = \sum_{m=1}^{\infty} \sum_{n=1}^{\infty} d_{mn} \varphi_{mn}(x, y) \quad (4.7)$$

The same kind of modal series can also be applied for the excitation force,

$$F(x, y) = \sum_{m=1}^{\infty} \sum_{n=1}^{\infty} F_{mn} \varphi_{mn}(x, y) \quad (4.8)$$

where F_{mn} is the density of the generalized force for mode (m, n) .

Substituting Eq.(4.7) and Eq.(4.8) into Eq.(4.6), this can then be written as

$$\begin{aligned} \rho \omega^2 \sum_{m=1}^{\infty} \sum_{n=1}^{\infty} d_{mn} \varphi_{mn}(x_0, y_0) + \frac{j\rho\omega}{z_h} \sum_{m=1}^{\infty} \sum_{n=1}^{\infty} [m(\omega_{mn}^2 - \omega^2) d_{mn} - F_{mn}] \varphi_{mn}(x_0, y_0) = \\ \int_{S_p} \sum_{m=1}^{\infty} \sum_{n=1}^{\infty} [m(\omega_{mn}^2 - \omega^2) d_{mn} - F_{mn}] \varphi_{mn}(x, y) \frac{\partial^2 G}{\partial z \partial z_0}(x, x_0, y, y_0, z = z_0 = 0) dx dy \end{aligned} \quad (4.9)$$

where ω_{mn} is the resonance frequency for a single mode defined by

$$\omega_{mn} = k_{mn}^2 \sqrt{\left(\frac{B}{m}\right)} \quad (4.10)$$

where k_{mn} denotes the modal wave number of mode (m, n) , which for a simply supported plate is given by

$$k_{mn} = \sqrt{\left(\frac{m\pi}{a}\right)^2 + \left(\frac{n\pi}{b}\right)^2} \quad (4.11)$$

and where the modes φ_{mn} satisfy

$$B \nabla^4 \varphi_{mn}(x, y) = m\omega_{mn}^2 \varphi_{mn}(x, y) \quad (4.12)$$

If the mode shape of the simply supported plate, say φ_{mn} is defined as

$$\varphi_{mn}(x, y) = \sin\left(\frac{m\pi x}{a}\right) \sin\left(\frac{n\pi y}{b}\right) \quad (4.13)$$

using the orthogonality relationship, one can obtain

$$\int_{S_p} \varphi_{mn} \varphi_{pq} dS_p = \frac{S_p}{4} \delta_{mp} \delta_{nq} \quad (4.14)$$

where δ is the Kronecker delta.

For the case of a simply supported plate, applying the orthogonality relationship from Eq.(4.14) to Eq.(4.9) yields

$$\begin{aligned} \rho\omega^2 \frac{S_p}{4} d_{pq} + \frac{j\omega\rho}{z_h} (m(\omega_{pq}^2 - \omega^2) d_{pq} - F_{pq}) \\ = \sum_{m=1}^{\infty} \sum_{n=1}^{\infty} (m(\omega_{mn}^2 - \omega^2) d_{mn} - F_{mn}) C_{pqmn} \end{aligned} \quad (4.15)$$

where d_{pq} is the modal complex displacement amplitude, F_{pq} is the modal excitation force and $C_{pqmn}=C_{mnpq}$ are the acoustical cross-modal coupling terms. To include the effect of damping into the sound radiation calculation, the plate natural frequency ω_{mn}^2 is replaced by $\omega_{mn}^2(1 + j\eta)$.

After re-arranging Eq.(4.15), its solution in terms of vectors and matrices can be written as

$$\begin{aligned} [C_{mnpq}] \{m(\omega_{mn}^2 - \omega^2) d_{mn}\} - \rho\omega^2 \frac{S_p}{4} [I] \{d_{mn}\} - \frac{j\omega\rho}{z_o} \frac{S_p}{4} [I] \{m(\omega_{mn}^2 - \omega^2) d_{mn}\} \\ = [C_{mnpq}] \{F_{mn}\} - [I] \frac{j\omega\rho}{z_h} \frac{S_p}{4} \{F_{mn}\} \end{aligned} \quad (4.16)$$

where $[I]$ is the $mn \times mn$ identity matrix and $\{\}$ denotes a column vector.

Multiplying by $[C_{mnpq}]^{-1}$ yields

$$\begin{aligned} [I] \{m(\omega_{mn}^2 - \omega^2) d_{mn}\} - \rho\omega^2 \frac{S_p}{4} [C_{mnpq}]^{-1} \left([I] \{d_{mn}\} + \frac{j\omega\rho}{z_h} [I] \{(\omega_{mn}^2 - \omega^2) d_{mn}\} \right) \\ = \left([I] - \frac{j\omega\rho}{z_h} \frac{S_p}{4} [C_{pqmn}]^{-1} \right) \{F_{mn}\} \end{aligned} \quad (4.17)$$

By neglecting the cross-modal coupling contributions in the sound radiation as in [8], the equation can be approximated by

$$\begin{aligned}
& m_{pq}(\omega_{pq}^2 - \omega^2)d_{pq} - \rho\omega^2 \left(\frac{S_p}{4}\right)^2 \frac{1}{C_{pqpq}} \left(1 + \frac{4jm_{pq}}{S_p\omega z_h}(\omega_{pq}^2 - \omega^2)\right) d_{pq} \\
& = \left(1 - \frac{j\omega\rho S_p}{z_h} \frac{1}{4 C_{pqpq}}\right) \hat{F}_{pq}
\end{aligned} \tag{4.18}$$

where $m_{pq} = m(S_p/4)$ and $\hat{F}_{pq} = F_{pq}(S_p/4)$ are the generalized mass and the generalized force respectively. The case of the unperforated, unbaffled plate can be recovered by introducing very large z_h .

Eq.(4.18) can be solved to find the complex displacement amplitude of mode (p, q) , d_{pq} . The plate velocity for each mode can be written as

$$v_{pq}(x, y) = \frac{\partial w}{\partial t} = j\omega d_{pq} \varphi_{pq}(x, y) \tag{4.19}$$

where φ_{pq} is the value of the corresponding mode shape function.

The space average mean square velocity of a mode can be expressed as

$$\langle v_{pq}^2 \rangle = \frac{1}{2S_p} \int_{S_p} |v_{pq}(x, y)|^2 dx dy \tag{4.20}$$

Substituting Eq.(4.19) for the case of a simply supported plate gives

$$\langle v_{pq}^2 \rangle = \frac{\omega^2}{8} |d_{pq}|^2 \tag{4.21}$$

As for the case of an unbaffled plate [8], the acoustic pressure is determined from the pressure difference $\Delta p(x, y)$ between the two sides of the plate surface. The total radiated sound power is defined as

$$W = \frac{1}{2} \int_{S_p} \Re \left\{ \sum_{p=1}^{\infty} \sum_{q=1}^{\infty} \Delta p(x, y) v_{pq}^*(x, y) \right\} dS_p \tag{4.22}$$

To obtain a convenient calculation, the pressure difference $\Delta p(x, y)$ can also be written as a sum of plate mode shapes

$$\Delta p(x, y) = \sum_{m=1}^{\infty} \sum_{n=1}^{\infty} p_{mn} \varphi_{mn}(x, y) \tag{4.23}$$

where p_{mn} are the corresponding amplitudes.

Therefore by using the orthogonality relationship from Eq.(4.14), the radiated sound power can be written as

$$\begin{aligned} W &= \frac{1}{2} \int_{S_p} \Re \left\{ \sum_{m=1}^{\infty} \sum_{n=1}^{\infty} p_{mn} \varphi_{mn} \times (j\omega) \sum_{p=1}^{\infty} \sum_{q=1}^{\infty} d_{pq}^* \varphi_{pq} \right\} dS_p \\ &= \frac{\omega S_p}{2} \frac{1}{4} \Re \left\{ j \sum_{p=1}^{\infty} \sum_{q=1}^{\infty} p_{pq} d_{pq}^* \right\} \end{aligned} \quad (4.24)$$

The effect of the perforation on the sound power is contained within the complex displacement amplitude, d_{pq} .

Substituting Eq.(4.23), Eq.(4.1) can then be written as

$$\begin{aligned} &\sum_{m=1}^{\infty} \sum_{n=1}^{\infty} m(\omega_{mn}^2 - \omega^2) d_{mn} \varphi_{mn}(x, y) \\ &= \sum_{m=1}^{\infty} \sum_{n=1}^{\infty} F_{mn} \varphi_{mn}(x, y) + \sum_{m=1}^{\infty} \sum_{n=1}^{\infty} p_{mn} \varphi_{mn}(x, y) \end{aligned} \quad (4.25)$$

Again, applying the orthogonality relationship yields

$$m(\omega_{pq}^2 - \omega^2) d_{pq} = F_{pq} + p_{pq} \quad (4.26)$$

Eliminating p_{pq} in Eq.(4.24) using Eq.(4.26)

$$W = \frac{\omega S_p}{8} \Re \left\{ j \sum_{p=1}^{\infty} \sum_{q=1}^{\infty} (m(\omega_{pq}^2 - \omega^2) d_{pq} - F_{pq}) d_{pq}^* \right\} \quad (4.27)$$

Therefore the total radiation efficiency σ can be found from

$$\sigma = \frac{W}{\rho c S_p \sum_{p=1}^{\infty} \sum_{q=1}^{\infty} \langle v_{pq}^2 \rangle} \quad (4.28)$$

This is the average radiation efficiency which is also defined as a summation over the contributions of modes (modal summation approach).

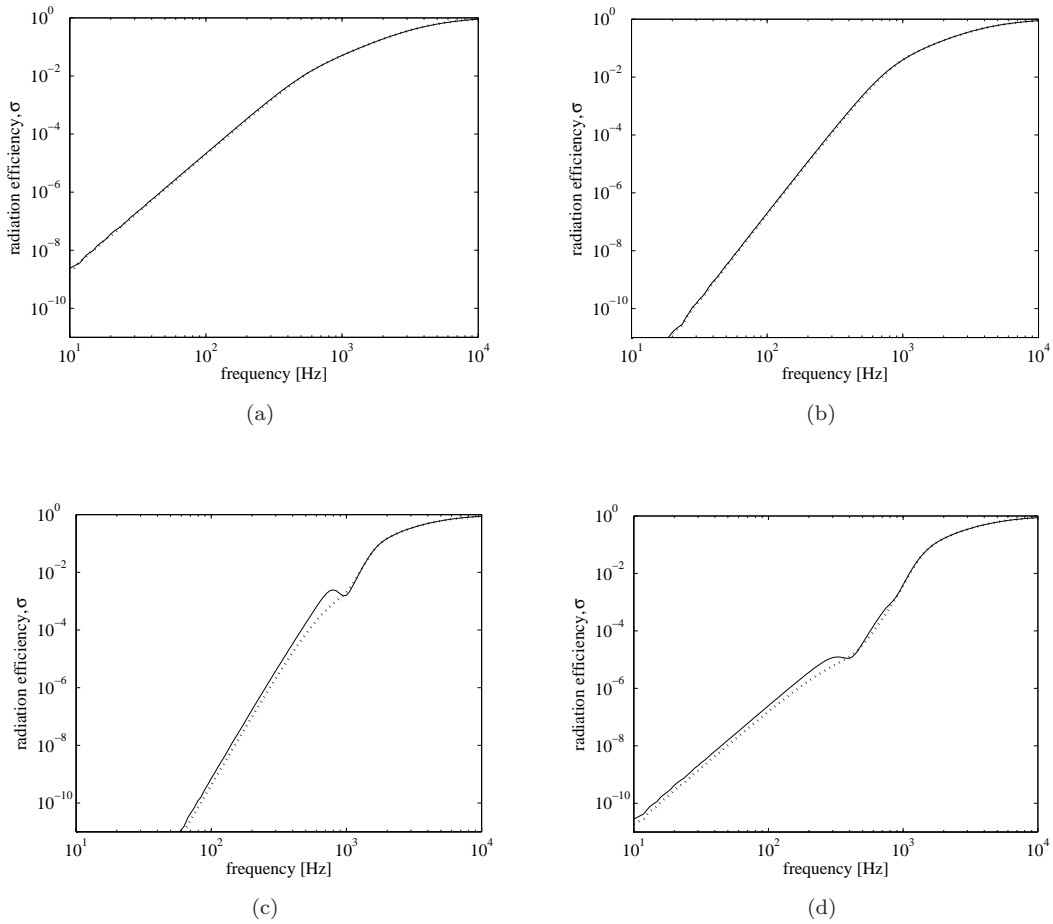


FIGURE 4.2: Comparison between the exact (—) and approximated calculation (···) of (a) mode (1,1), (b) mode (1,2), (c) mode (2,4) and (d) mode (3,3) ($0.65 \times 0.5 \times 0.003$ m aluminium plate with $\eta = 0.1$; $d_o = 10$ mm, $\tau = 40\%$).

4.2 Results

Figure 4.2 shows a comparison between the calculation of the radiation efficiency for modes (1,1), (1,2), (2,4) and (3,3) using Eq.(4.17) involving the full matrix $[C_{pqmn}]$ and the one using Eq.(4.18), based on neglecting cross-modal terms.

For calculating the results using Eq.(4.17), i.e. using the full matrix of C_{pqmn} , a total of 49×49 modes are included in each calculation. In each case only modes of the same parity are included as other terms are zero. In this section, the calculation using Eq.(4.17) is called the exact calculation, whereas the calculation using Eq.(4.18) is called the approximate calculation.

For modes (1,1) and (1,2), the approximate result has a very close agreement with the exact result. Differences occur for modes (2,4) and (3,3) below the natural frequency of each mode. This is the effect of the cross-modal coupling which is greater in the higher

modes. In the unbaffled plate case, the cross-modal terms do not completely converge to zero as they do for the baffled plate case, even though all possible force positions have been averaged. However, using only the self-modal radiation from the approximate calculation is still considered to give quite good agreement with the results from the exact calculation, especially when the full modal summation is considered. Therefore, in the remainder of this section, the calculation of the radiation efficiency is carried out by using Eq.(4.18), i.e. neglecting the cross-modal coupling distribution.

Figure 4.3 presents the results of the modal and average radiation efficiencies of an unbaffled perforated plate with 40% perforation ratio and 10 mm diameter holes. The results show a curve which has the same trend of slope as obtained from the case of a perforated plate in an infinite perforated baffle, see Figure 3.2, particularly for the region below the first mode (40 dB/decade) and the corner mode region (20 dB/decade). However, the unbaffled plate has a lower radiation efficiency than that of the plate in the perforated baffle for most of the frequency range below the critical frequency, as shown in Figure 4.4. As the perforation ratio increases, the radiation efficiency of the perforated plate in a perforated baffle becomes very similar to that of the unbaffled perforated plate. At high perforation ratio, the contribution of the baffle to the radiated sound is no longer significant. This is confirmed in Figure 4.5 which shows the differences of the radiation efficiencies $\Delta\sigma$ for no baffle and a perforated baffle on a dB scale. This shows that for a 10 mm hole diameter and 60% perforation ratio, the difference is only around 1 dB. Therefore with very high perforation ratio, the system with a perforated baffle can then be considered to be equivalent to the unbaffled perforated plate.

Figure 4.6 compares the results with the unperforated unbaffled plate. Perforation yields a constant reduction over the frequencies up to the corner mode region (at 450 Hz in this case). The effect then reduces as frequency increases. This can be explained as the impedance of the hole is proportional to frequency. Therefore at high frequency, the fluid in the holes has very high impedance and hence behaves like a solid mass. This mass does not move to suppress the fluid from the volume sources adjacent to the hole. The cancellation of radiated sound is thus not effective.

Figure 4.7 and Figure 4.8 present the effect of perforation for constant hole diameter and constant perforation ratio, respectively. These show that, for the case of the unbaffled perforated plate, the effect of perforation is almost independent of the frequency below the edge mode region and then increases in the edge mode region as the frequency increases. Results for different thicknesses and dimensions are presented in Figure 4.9. Unlike the perforated baffled case, the results show that the effect of perforation in the unbaffled perforated case depends on both the plate thickness (see Figure 4.9(a), 4.9(b)) and on the plate dimension (see Figure 4.9(c), 4.9(d)).

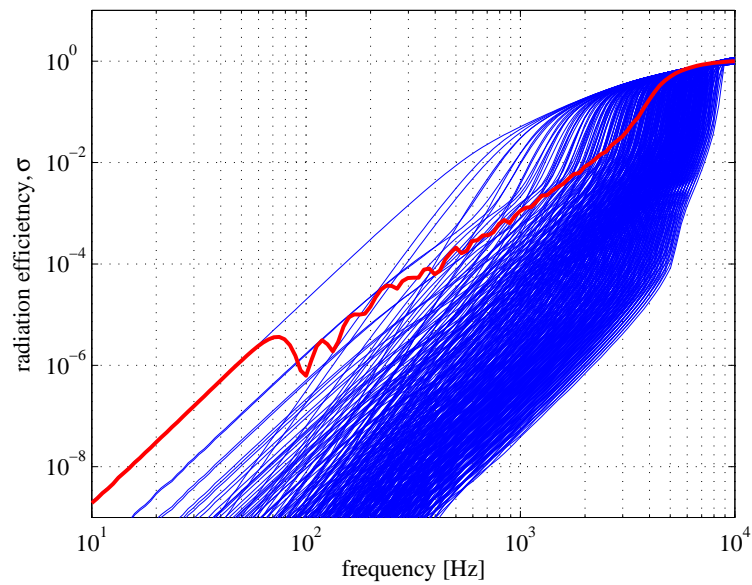


FIGURE 4.3: Modal and average radiation efficiency of a simply supported rectangular unbaffled perforated plate ($0.65 \times 0.5 \times 0.003$ m aluminium plate with $\eta = 0.1$; $d_o = 10$ mm, $\tau = 40\%$):—, modal radiation efficiency; —, average radiation efficiency.

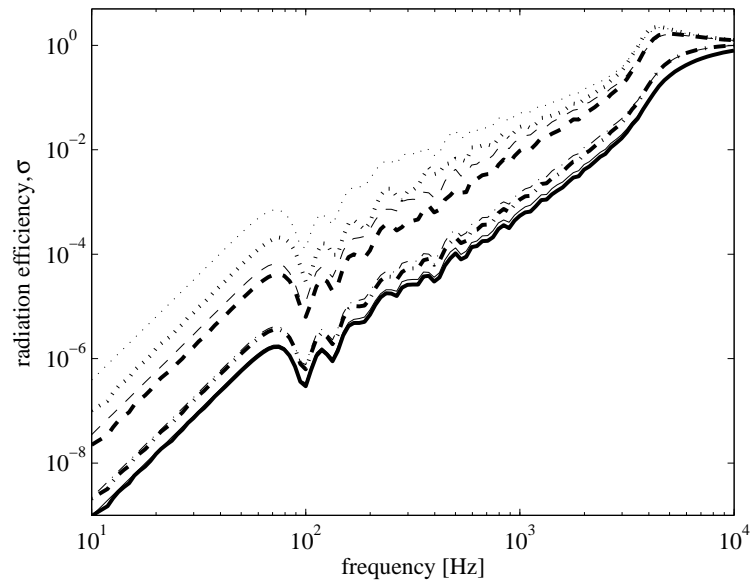


FIGURE 4.4: Average radiation efficiency of simply supported rectangular perforated plates in a perforated baffle (thin line) and unbaffled (thick line) ($0.65 \times 0.5 \times 0.003$ m aluminium plate with $\eta = 0.1$; $d_o = 10$ mm): \cdots $\tau=3\%$, $---$ $\tau=10\%$, $- \cdot -$ $\tau=40\%$ mm, $—$ $\tau=60\%$.

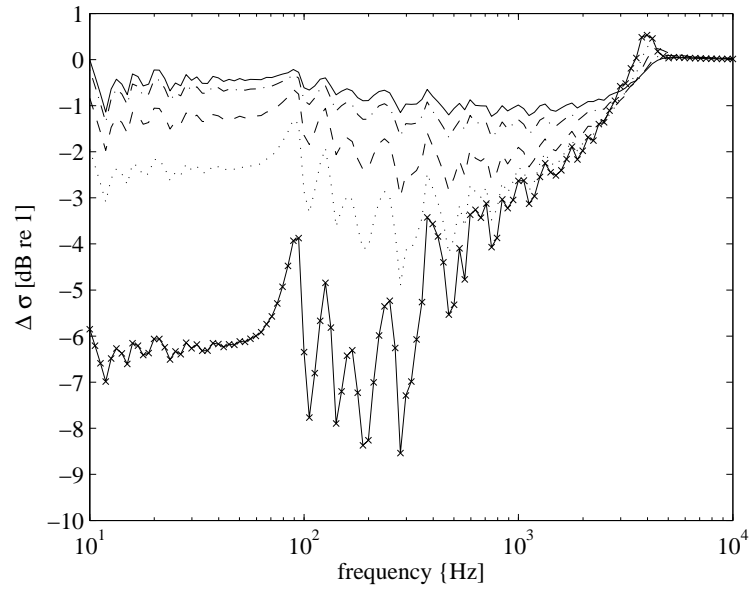


FIGURE 4.5: Radiation efficiency difference of a perforated plate in a perforated baffle and an un baffled plate) ($0.65 \times 0.5 \times 0.003$ m aluminium plate with $\eta = 0.1$; $d_o = 10$ mm): \times — $\tau=3\%$, \cdots $\tau=10\%$, $--$ $\tau=20\%$, $-\cdot-$ $\tau=40\%$ mm, $---$ $\tau=60\%$.

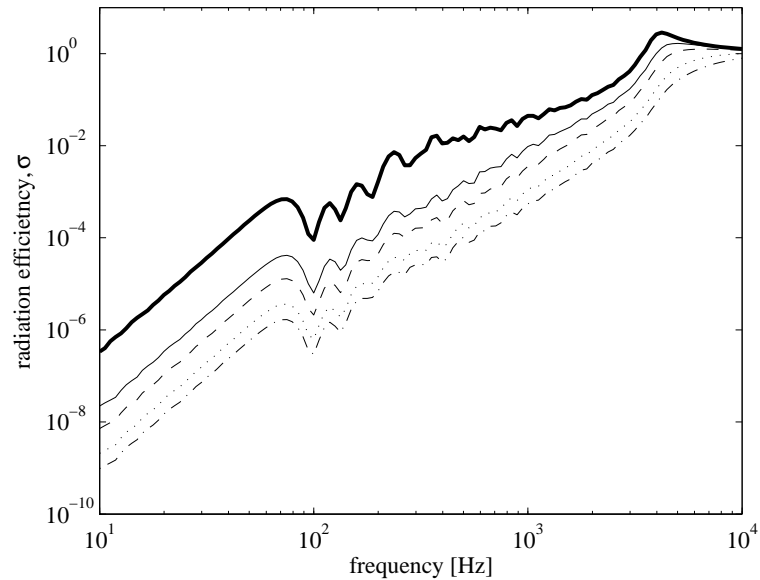


FIGURE 4.6: Average radiation efficiency of a simply supported rectangular un baffled perforated plate ($0.65 \times 0.5 \times 0.003$ m aluminium plate with $\eta = 0.1$, $d_o = 10$ mm; — unperforated, $---$ $\tau=10\%$, $--$ $\tau=20\%$, \cdots $\tau=40\%$ mm, $-\cdot-$ $\tau=60\%$).

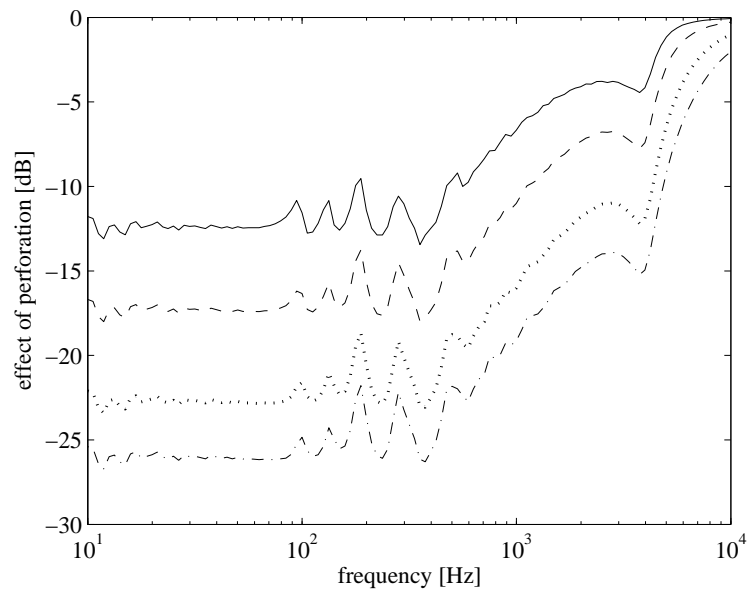


FIGURE 4.7: Effect of perforation on sound power radiation of a simply supported rectangular perforated un baffled plate ($0.65 \times 0.5 \times 0.003$ m aluminium plate with $\eta = 0.1$, $d_o = 10$ mm; — $\tau=10\%$, -- $\tau=20\%$, $\cdots\tau=40\%$ mm, -·- $\tau=60\%$).

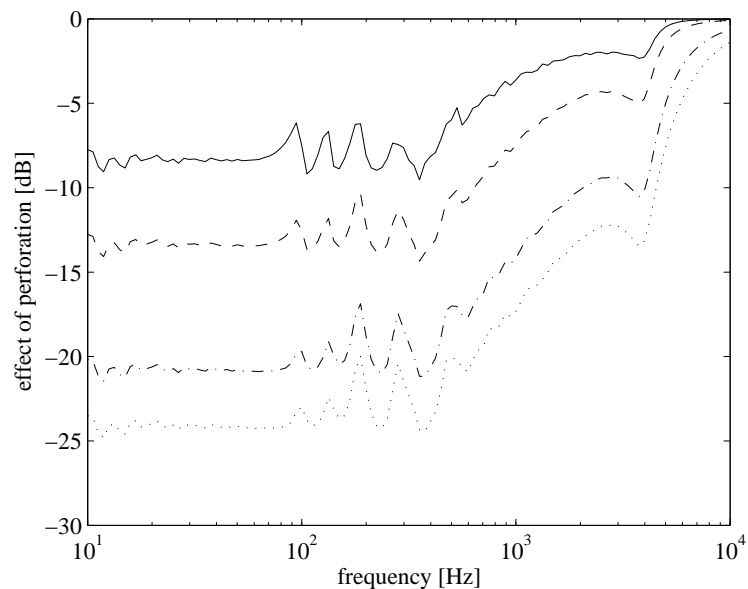


FIGURE 4.8: Effect of perforation on sound power radiation of a simply supported rectangular perforated un baffled plate ($0.65 \times 0.5 \times 0.003$ m aluminium plate with $\eta = 0.1$; $\tau=20\%$: $d_o =$ — 50 mm, -- 20 mm, -·- 5 mm, \cdots 2 mm).

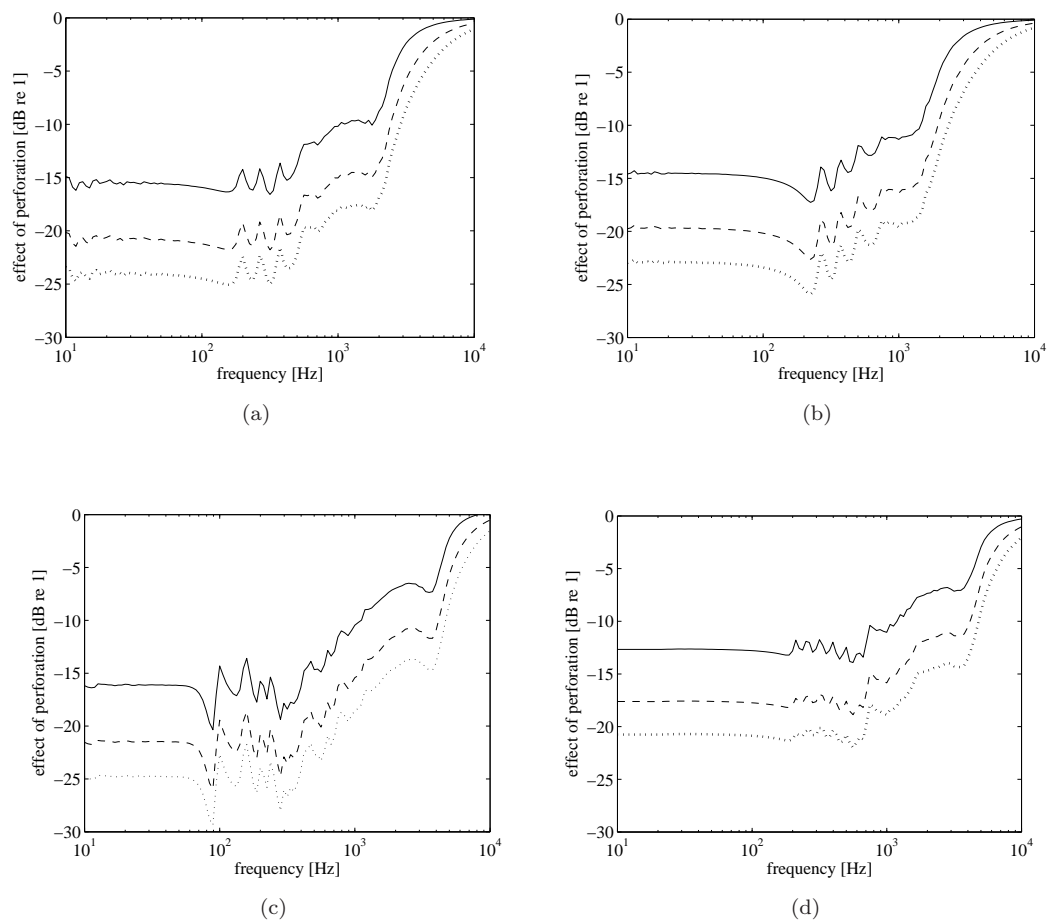


FIGURE 4.9: Effect of perforation on sound power radiation of a simply supported rectangular perforated unbaffled plate for different thicknesses; (a) $0.65 \times 0.5 \times 0.006$ m, (b) $0.65 \times 0.5 \times 0.008$ m and different dimensions; (c) $0.8 \times 0.4 \times 0.003$ m, (d) $0.9 \times 0.2 \times 0.003$ m (aluminium plate with $\eta = 0.1$; $d_o = 10$ mm, $\tau =$ — 20%, -- 40%, \cdots 60%).

Figure 4.10 shows a comparison of the radiation index ($10 \log_{10} \sigma$) from the analytical calculation with that from the measurements made by Pierri [19] for 0.3×0.3 m steel plates with 1.22 mm thickness. The results are plotted against $1/3$ octave band centre frequencies. The damping loss factor in the calculations is chosen to be very low, i.e. $\eta = 0.001$. A very good agreement between the theoretical and the measurement results is achieved although below 800 Hz, the measured radiation efficiencies are greater than the predictions by about 3 – 4 dB. This is probably due to the high variability of the radiation efficiency in the corner mode region as the force was only applied at one location on the plate in the experiment [19]. This variability due to the excited point force positions has been described in [18, 20]. Moreover, the background noise in this region could also have a significant effect. Above 1 kHz the measured data is lower than than the prediction for the plate with 41.5% perforation ratio. However, it still follows the same trend as the prediction.

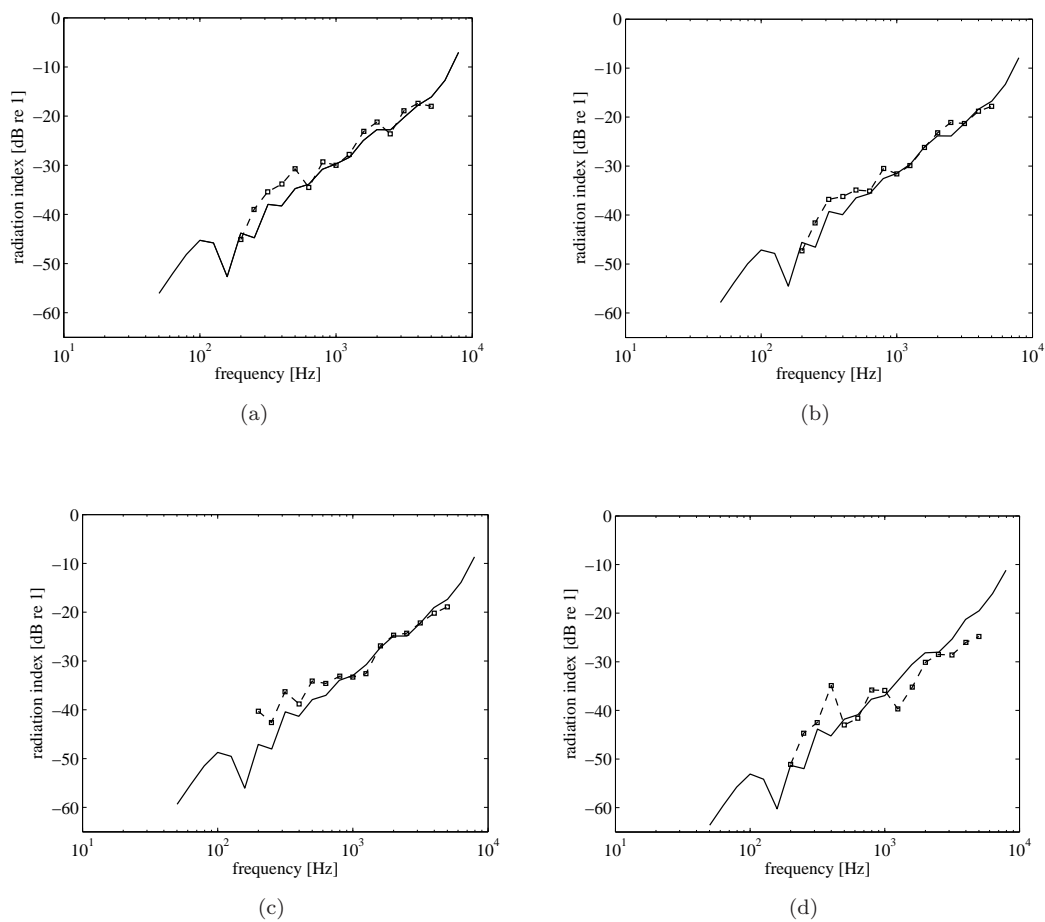


FIGURE 4.10: Comparison of the radiation index from analytical calculation (—) with that of the measurement from Pierrri in 1/3 octave bands (---) ($0.3 \times 0.3 \times 0.0012$ m un baffled steel plate with $\eta = 0.001$): (a) $d_o=5.6$ mm, $\tau=5.7\%$; (b) $d_o=7.1$ mm, $\tau=9.4\%$; (c) $d_o=8.8$ mm, $\tau=14.1\%$; (d) $d_o=15$ mm, $\tau=41.5\%$.

Figure 4.11 plots the effect of perforation for the same plates. It also shows a good agreement with the prediction, except for the 41.5% perforation ratio plate where differences of up to 10 dB are found at 400 Hz and 1.25 kHz.

4.3 Approximate formula for IL at low frequency

Figure 4.12 plots the effect of perforation against h for different plate thickness. The curves collapse together with the same slope in the edge mode region where the insertion loss is dependent on h . Below the edge mode region, the results are independent of h but vary with plate on dimensions and perforation ratio.

As the effect of perforation ratio ($-IL$) for the un baffled perforated plate shows constant values at low frequency, at least up to end of the corner mode region, an approximate

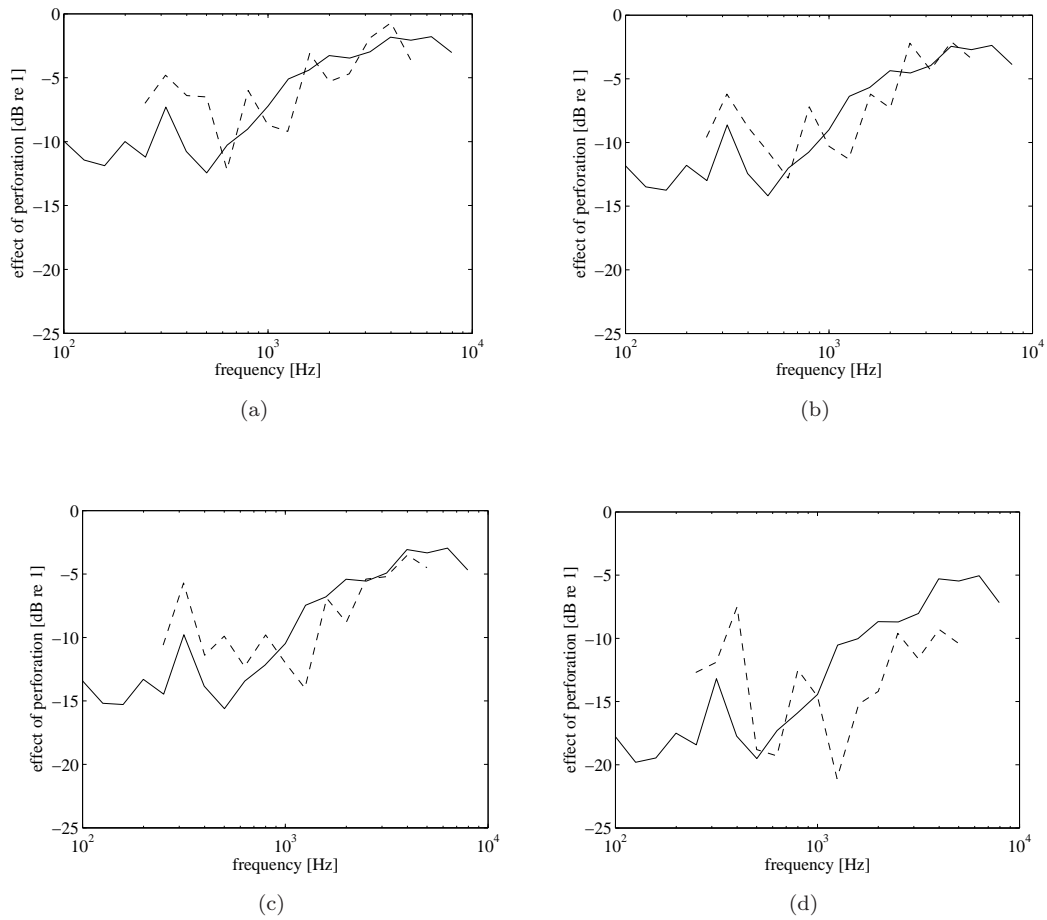


FIGURE 4.11: Comparison of the effect of perforation from analytical calculation (—) with that of the measurement from Pierri in 1/3 octave bands (---) ($0.3 \times 0.3 \times 0.0012$ m unbaffled steel plate with $\eta = 0.001$): (a) $d_o = 5.6$ mm, $\tau = 5.7\%$; (b) $d_o = 7.1$ mm, $\tau = 9.4\%$; (c) $d_o = 8.8$ mm, $\tau = 14.1\%$; (d) $d_o = 15$ mm, $\tau = 41.5\%$.

formula can be developed to determine the effect of perforation ratio in this frequency range.

Figure 4.13 plots the effect of perforation at low frequency for plates with the same dimensions but different thickness and perforation ratio to show the increment of $-IL$ as the plate thickness increases. It is shown that the perforation of the thinner plate has a greater effect of reducing the sound radiation. The result also shows that the trend has a dependency of 17.8 dB/decade. Hence it can be determined as a function of the non-dimensional acoustic reactance h written as

$$-IL_{ubf,h} = 17.78 \log_{10} \left(\frac{h}{k} \right) + 5.14, \quad k < k_e \quad (4.29)$$

where $IL_{ubf,h}$ is the insertion loss of the unbaffled perforated plate at very low frequency,

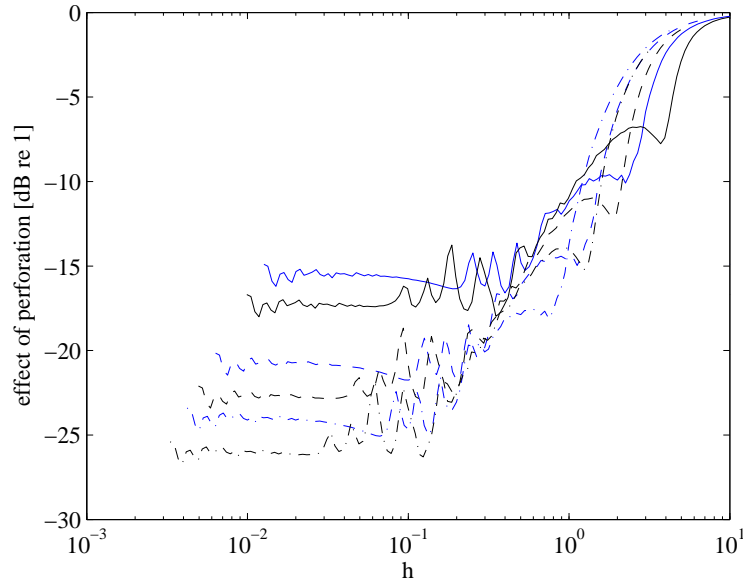


FIGURE 4.12: Effect of perforation on sound power radiation of a simply supported rectangular perforated, un baffled plate plotted against h ($0.65 \times 0.5 \times 0.003$ m (black line), $0.65 \times 0.5 \times 0.006$ m (blue line)); aluminium plate with $\eta = 0.1$, $d_o = 10$ mm; $\tau =$ — 20%, — — 40%, - · - 60%).

i.e. in the dipole and the corner mode regions, as a function of h (thickness, perforation ratio and hole diameter) and $k_e = 2\pi f_e/c$ is the wavenumber corresponding to the starting frequency of the edge mode region.

The effect of perforation at low frequency for different dimensions with the same plate thickness is shown in Figure 4.14 for the perforation ratio of 20% and 40%. For the 20% perforation ratio, the function of the curve in terms of the plate dimensions can be written as

$$-IL_{ubf,dimension} = -17.37 \log_{10} \left(\frac{ab}{a+b} \right) + 7.94, \quad k < k_e \quad (4.30)$$

where $a \times b$ is the plate area¹. The 40% perforation ratio can be regarded to have the same slope of Eq.(4.30).

Both equations (Eq.(4.29) and Eq.(4.30)) can be combined to give a general equation for the insertion loss at low frequency expressed as

$$-IL_{ubf} = -17.37 \log_{10} \left(\frac{ab}{a+b} \right) + 17.78 \log_{10} \left(\frac{h}{k} \right) - 4.36, \quad k < k_e \quad (4.31)$$

¹The results were also plotted against ab , a/b and $a+b$ but these did not yield a consistent relationship as here.

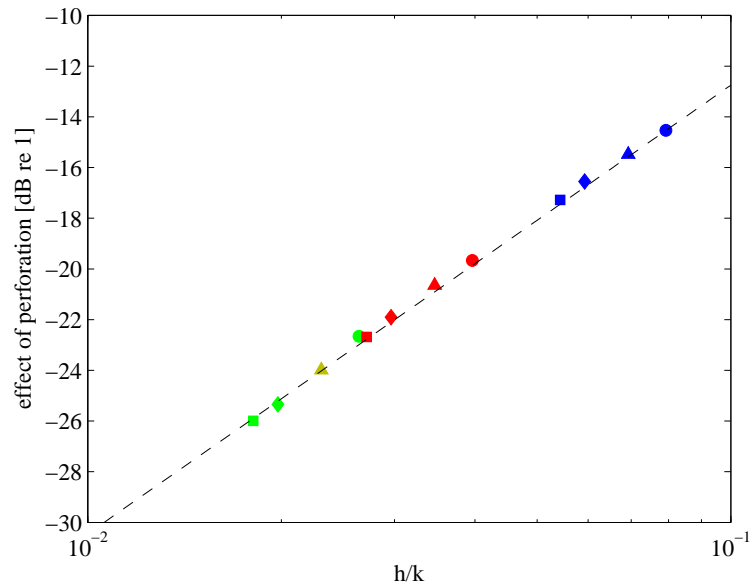


FIGURE 4.13: Effect of perforation on sound power radiation of a simply supported rectangular perforated un baffled plate at low frequency asymptote for different thickness (\square : $0.65 \times 0.5 \times 0.003$ m, \diamond : $0.65 \times 0.5 \times 0.004$ m, \triangle : $0.65 \times 0.5 \times 0.006$ m, \circ : $0.65 \times 0.5 \times 0.008$ m aluminium plate with $\eta = 0.1$; $\tau=20\%$ (blue), $\tau=40\%$ (red), $\tau=60\%$ (green)).

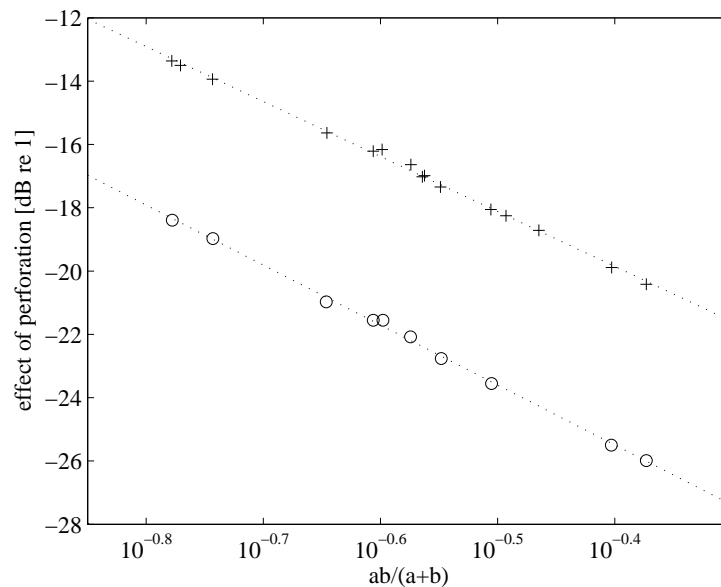


FIGURE 4.14: Effect of perforation on sound power radiation of a simply supported rectangular perforated un baffled plate at low frequency asymptote for various plate dimensions ($t = 0.003$ m, aluminium plate with $\eta = 0.1$; $+$ = 20%, \circ = 40%).

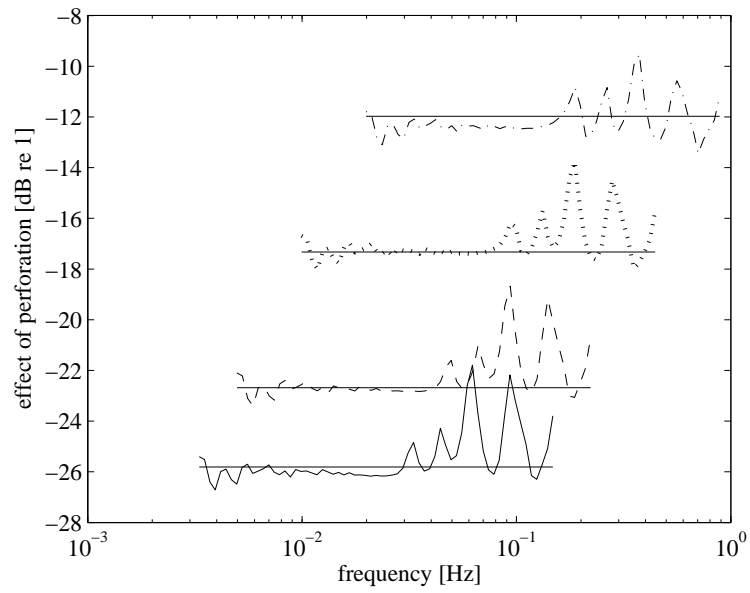


FIGURE 4.15: Comparison of exact and approximated (thick line) insertion gain ($-IL$) of a simply supported rectangular perforated, un baffled plate: $0.65 \times 0.5 \times 0.003$ m; $- \cdot - \tau = 10\%$, $\dots \tau = 20\%$, $-- \tau = 40\%$, $- \tau = 60\%$ (aluminium plate with $\eta = 0.1$, $d_o = 10$ mm).

Figures 4.15 and 4.16 show the effect of perforation below the edge mode frequency (wavenumber k_e), to test the validity of Eq.(4.31) by varying perforation ratio, plate dimension and thickness. It is shown that it gives good agreement at very low frequency.

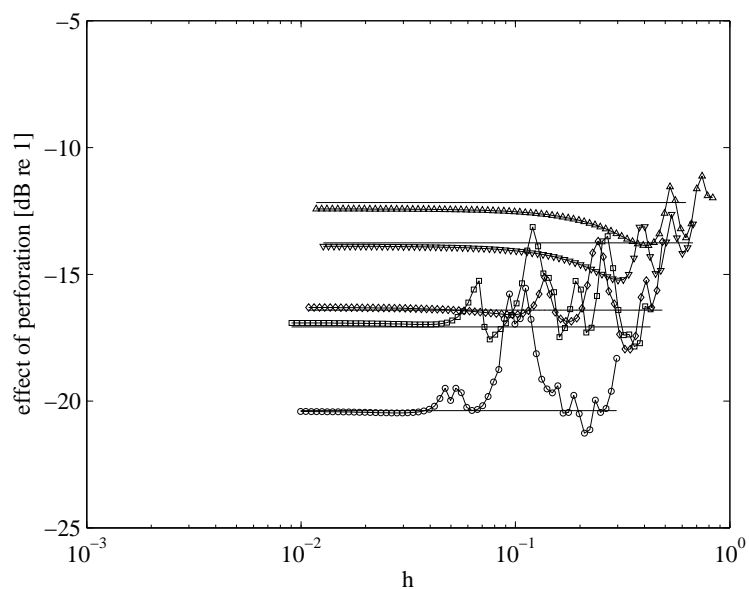


FIGURE 4.16: Comparison of exact (marked) and approximated insertion gain ($-IL$) of a simply supported rectangular perforated, un baffled plate: $\tau=20\%$; $\nabla 0.39 \times 0.3 \times 0.005$ m, $\triangle 0.52 \times 0.4 \times 0.006$ m, $\diamond 0.7 \times 0.45 \times 0.004$ m, $\square 0.65 \times 0.4 \times 0.002$ m, $\circ 0.9 \times 0.8 \times 0.003$ m) (aluminium plate with $\eta = 0.1$, $d_o = 10$ mm).

Chapter 5

Sound Radiation from a Baffled Plate Modelled by Discrete Sources

In the previous chapters, the assumption is made that the array of holes can be replaced by a uniform layer of acoustic impedance at the surface of the plate. For this to be valid, the distance between the holes must be short enough compared with the acoustic wavelength. However, the effect is not obvious in the models because the perforation ratio is a parameter defined without necessarily knowing the hole position and also the distance between holes. As already mentioned in Section 2.3, there should be a frequency limit where the continuous impedance assumption is breached when the hole distance is far apart compared with the acoustic wavelength.

To investigate this phenomenon, a continuous baffled source can be modelled by replacing it with an array of sources. Thus a perforated plate can be modelled by an array of sources, some representing the plate and others the holes. The acoustic pressure for each source due to the other sources is calculated numerically. This discrete source model is attractive as the hole configuration can be arbitrarily set and the hole distance is known.

5.1 Discrete Version of Rayleigh Integral

The well-known Rayleigh integral [9] can be used to calculate the sound pressure at any point of observation due to a vibrating plate set in an infinite rigid baffle. The equation can be written as

$$p(\mathbf{x}) = -2 \int_s g(\mathbf{x}|\mathbf{x}_s) \left(\frac{\partial p(\mathbf{x})}{\partial n} \right)_S dS \quad (5.1)$$

where $\mathbf{x} = (x, y)$ and S denotes the surface area of the plate. The first term of the integrand is the free-field Green's function which is the sound pressure contribution at \mathbf{x} due to the radiation of a point monopole source of area dS at \mathbf{x}_s . Since $U_p = (-1/j\rho ck)\partial p/\partial n$ and $g = e^{-jkR}/4\pi R$, thus

$$p(\mathbf{x}) = \frac{j\rho ck}{2\pi} \int_s U_p(\mathbf{x}_s) \frac{e^{-jkR}}{R} dS \quad (5.2)$$

where $R = |\mathbf{x} - \mathbf{x}_s|$.

The Rayleigh integral requires that the normal velocity is known over the whole surface plate area. For the case of a moving piston, the normal velocity is uniform across the plate surface

$$U_p(\mathbf{x}_s) = U_n \quad (5.3)$$

For bending of a rectangular plate having dimensions $a \times b$ and assuming simply supported edges, the velocity can be written as the sum of modal vibration contributions given by

$$U_p(\mathbf{x}_s) = \sum_{m=1}^{\infty} \sum_{n=1}^{\infty} u_{mn} \sin\left(\frac{m\pi x}{a}\right) \sin\left(\frac{n\pi y}{b}\right) \quad (5.4)$$

where u_{mn} is the complex velocity amplitude of mode (m, n) . For a point force excitation at (x_0, y_0) , it can be defined as [21]

$$u_{mn} = \frac{2j\omega F}{[\omega_{mn}^2(1 + j\eta) - \omega^2]M} \sin\left(\frac{m\pi x_0}{a}\right) \sin\left(\frac{n\pi y_0}{b}\right) \quad (5.5)$$

where F is the force amplitude, ω_{mn} is the natural frequency, η is the hysteretic damping loss factor, and M is the plate mass.

The Rayleigh integral can next be written in discrete form as a sum over discrete source regions. Concerning the rectangular plate in the xy coordinate plane, the sources are defined by dividing the plate into a set of grid points. The spacings between points are dx in the x direction and dy in the y direction. The small element $dS = dxdy$ thus becomes a discrete monopole source of the plate. This requires that the elemental source size must be much smaller compared with the acoustic wavelength ($k dx \ll 1, k dy \ll 1$).

Discretizing the Rayleigh integral yields

$$p(\mathbf{x}) = \frac{j\rho ck}{2\pi} \sum_j U_p(\mathbf{x}_j) \frac{e^{-jkR}}{R} dxdy \quad (5.6)$$

where $R = |\mathbf{x} - \mathbf{x}_j|$. However when \mathbf{x} lies on the surface ($\mathbf{x} = \mathbf{x}_i$) the integrand is singular for $i = j$. To solve the integral over element i , another approximation corresponding to the pressure distribution on the plate surface is needed. Morse and Ingard [11] give the total force per unit area (pressure) acting on a rectangular (almost square) piston moving with uniform velocity U_n . For a plate of dimensions $a \times b$ where $b \cong a$, the radiation impedance is expressed as

$$\frac{p}{U_n} = \frac{\rho c k^2}{16}(a^2 + b^2) + \frac{j 8 \rho c k}{9\pi} \left(\frac{a^2 + ab + b^2}{a + b} \right), \quad ka \ll 1 \quad (5.7)$$

Applying this to the elemental source dS and assuming a square piston, i.e. $a = dx = b = dy$, this reduces to

$$\frac{p}{U_n} = \rho c \left(\frac{k^2 dx^2}{8} + \frac{j 4k dx}{3\pi} \right), \quad k dx \ll 1 \quad (5.8)$$

Therefore the Rayleigh integral can be written in the form

$$\{p_i\} = \mathbf{M}_{ij} \{U_j\} \quad (5.9)$$

where

$$\mathbf{M}_{ij} = \begin{cases} \frac{j \rho c k}{2\pi} \left(\frac{e^{-jkR_{ij}}}{R_{ij}} \right) dx^2, & i \neq j \\ \rho c \left(\frac{k^2 dx^2}{8} + \frac{j 4k dx}{3\pi} \right), & i = j \end{cases}$$

The matrix \mathbf{M} is actually an impedance matrix since the acoustic impedance expresses the ratio of complex pressure to the associated particle velocity.

5.2 Impedance matrix

Consider an array of circular holes on a plate, as shown in Figure 5.1. Each hole can be considered to be an acoustic source with volume velocity $\pi d_o^2 U_h / 4$ where U_h is the fluid velocity in the hole and d_o is the diameter of the hole.

The pressure at any point on the plate surface can be written as a sum of the pressure contributions from the sources representing the plate and the holes. The pressure at source position i due to source j can be written as

$$p_i = \sum_j M_{ij} U_j \quad (5.10)$$

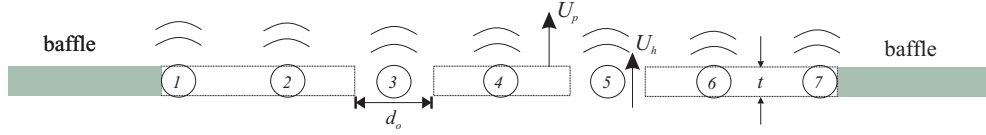


FIGURE 5.1: Analytical model of an array of discrete (monopole) sources for calculating the sound radiation of a perforated plate

where U_j is the velocity of source j which may represent the plate surface as the holes. M_{ij} can be written as a matrix, for example

$$\mathbf{M}_{ij} = \begin{pmatrix} M_{11} & \cdot & M_{13} & \cdot & M_{15} & \cdot & M_{17} \\ \cdot & \cdot & M_{23} & \cdot & M_{25} & \cdot & \cdot \\ M_{31} & M_{32} & M_{33} & M_{34} & M_{35} & M_{36} & M_{37} \\ \cdot & \cdot & M_{43} & \cdot & M_{45} & \cdot & \cdot \\ M_{51} & M_{52} & M_{53} & M_{54} & M_{55} & M_{56} & M_{57} \\ \cdot & \cdot & M_{63} & \cdot & M_{65} & \cdot & \cdot \\ M_{71} & \cdot & M_{73} & \cdot & M_{75} & \cdot & M_{77} \end{pmatrix} \quad (5.11)$$

In the present example, sources 3 and 5 correspond to the hole (see Figure 5.1). The matrix \mathbf{M}_{ij} can be rearranged to give

$$\mathbf{M} = \begin{pmatrix} \mathbf{M}_{p-p} & \mathbf{M}_{p-h} \\ \mathbf{M}_{h-p} & \mathbf{M}_{h-h} \end{pmatrix} \quad (5.12)$$

where $p-p$ refers to the pressure at a plate location due to plate sources, $p-h$ refers to the pressure at plate locations due to hole sources, etc.

The pressure and velocity can be partitioned into components at the plate and the holes giving

$$\begin{Bmatrix} p_p \\ p_h \end{Bmatrix} = \mathbf{M} \begin{Bmatrix} U_p \\ U_h \end{Bmatrix} \quad (5.13)$$

where $\{\}$ denotes a column vector.

The fluid velocity in the hole is defined from the acoustic impedance of the hole Z_h

$$U_f = -\frac{2p_h}{Z_h} \quad (5.14)$$

where $Z_h = \tau z_h$.

The model is developed for discrete, independent holes on the plate. Therefore, the acoustic impedance is no longer treated as a uniform specific acoustic impedance z_h across the plate surface as in Eq.(2.12).

As the fluid velocity in each hole may be represented by n_e monopole sources, the fluid velocity through the hole area must be averaged to the small element area dS of a monopole source to maintain its source strength. Thus

$$U_{fa} = U_f \left(\frac{\pi d_o^2/4}{n_e dS} \right) \quad (5.15)$$

As its direction is the opposite of the plate velocity direction, the velocity from the hole U_h is the relative velocity of the plate and of the fluid. It can be expressed as

$$U_h = U'_p + U_{fa} = U'_p - \frac{p_h}{2Z_h} \left(\frac{\pi d_o^2}{n_e dS} \right) \quad (5.16)$$

where U'_p is the plate velocity at the hole locations.

Both the pressure at the plate location and at the holes can then be written as

$$\{p_p\} = [M_{p-p}] \{U_p\} + [M_{h-p}] \{U_h\} \quad (5.17)$$

$$\{p_h\} = [M_{h-p}] \{U_p\} + [M_{h-h}] \{U_h\} \quad (5.18)$$

Substituting (5.16) into (5.18) and rearranging yields

$$\left[I + \frac{2M_{h-h}}{z_h} \right] \{p_h\} = ([M_{h-p} \quad M_{h-h}]) \{\bar{U}_p\} \quad (5.19)$$

where $\{\bar{U}_p\}$ is a vector containing the plate velocity at all locations including the plate (U_p) and the holes (U'_p) and I is the identity matrix.

Inverting the matrix on the left-hand side of (5.19) gives

$$\{p_h\} = \left[I + \frac{2M_{h-h}}{z_h} \right]^{-1} ([M_{h-p} \quad M_{h-h}]) \{\bar{U}_p\} \quad (5.20)$$

The pressure at the plate locations p_p can be obtained by substituting (5.20) into (5.16) to give U_h and then substituting into (5.17).

The total sound power of the plate is found from the sum over the contribution of all discrete sources

$$W = \frac{1}{2} \Re \left(\sum p_p U_p^* + \sum p_h U_h^* \right) dS \quad (5.21)$$

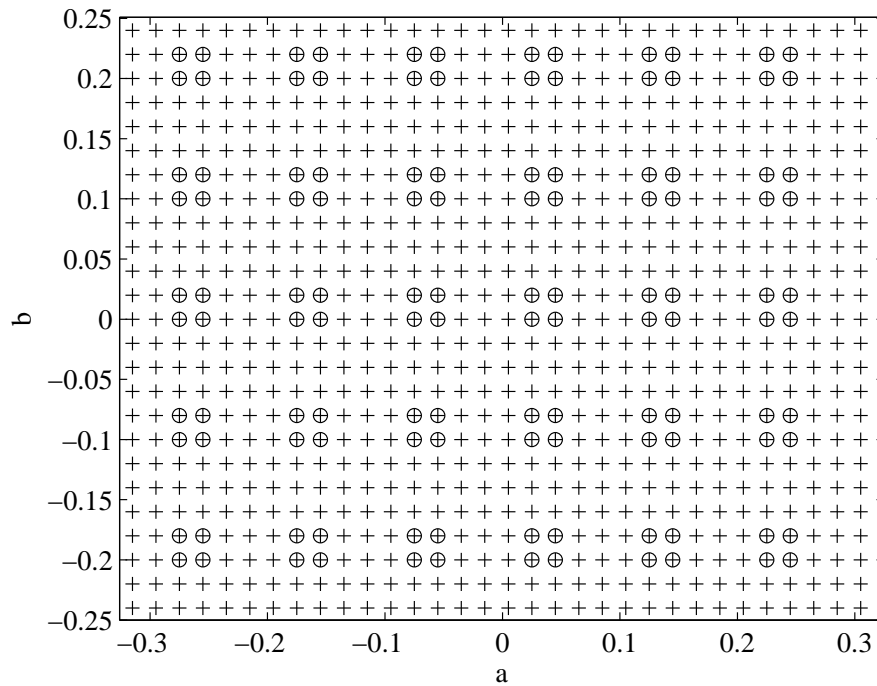


FIGURE 5.2: Example of the grid points (+) and the locations of 6×5 holes (o) on the plate (0.65×0.5 m) .

where dS is the small element of the plate area.

Finally, the radiation efficiency of the perforated plate can be written as

$$\sigma = \frac{2W}{\rho cab \langle \bar{U}_p^2 \rangle} \tag{5.22}$$

where $\langle \bar{U}_p^2 \rangle / 2$ is the spatially averaged mean square surface velocity of the plate.

5.3 Results

5.3.1 Radiation by a vibrating piston

The sound radiation by a perforated vibrating piston is calculated by using Eq.(5.3) for the uniform plate velocity. Figure 5.2 shows a plate of $0.65 \times 0.5 \times 0.003$ m with the grid points and the locations of the holes. With the elemental source spacing of $dx = dy = 0.02$ m, the number of elemental sources is 800. In this example, 30 holes are chosen where each hole is represent by four monopoles. The hole distance in the x or y axis is 0.1 m.

Figure 5.3 plots the results for various perforation ratios (different number of holes) with the hole diameter $d_o=4$ cm. It can be seen that the radiation efficiency reduces as the

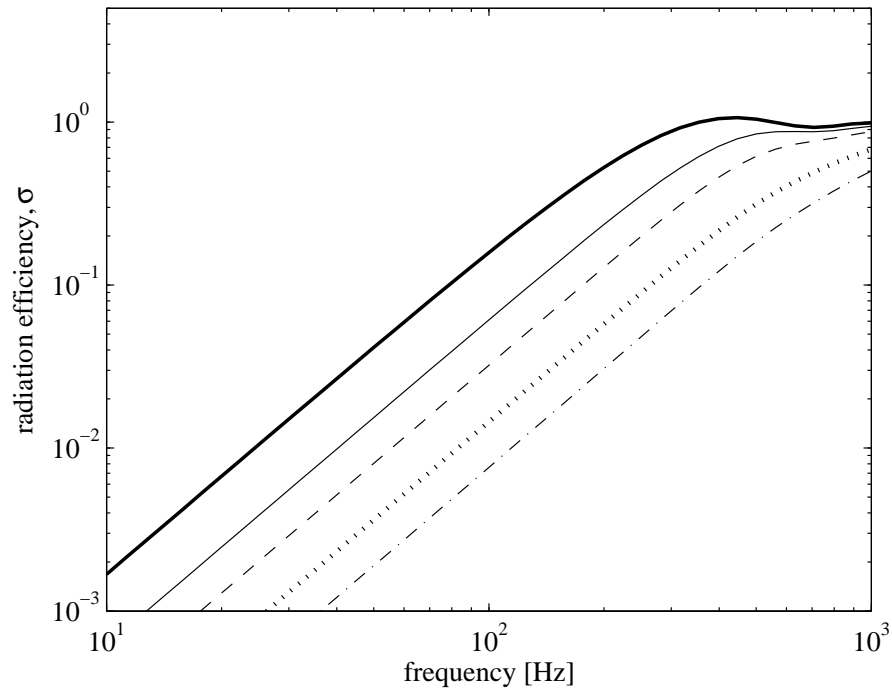


FIGURE 5.3: Radiation efficiency of a perforated baffled plate (rectangular piston) from discrete monopole sources: $0.65 \times 0.5 \times 0.003$ m, $d_o = 0.04$ m, $dx = 0.02$ m (— unperforated, $-\tau=6\%$, $--\tau=12\%$, $\cdots\tau=22\%$, $-\cdot-\tau=31\%$).

perforation ratio increases. The curves all have 20 dB/decade slope until they converge to unity. This proportionality to f^2 shows the characteristic of a monopole source. The results are not calculated up to very high frequency as this requires more elemental sources to ensure $k dx \ll 1$. This would take much greater calculation time. For the present case, the calculation of radiation efficiency up to 1 kHz (frequency resolution of 40 points per decade, spaced logarithmically) using MATLAB takes about 35 seconds. For comparisons, calculation for 1491 sources take 100 seconds (PC Pentium 4[®] 0.99 GB RAM). However to cover the frequency region up to 10 kHz would require at least 1.2×10^5 sources leading to a very large increase in computing time.

Figure 5.4 plots the results for various hole diameters with constant perforation ratio. It can be seen that the radiation efficiency (for constant perforation ratio) can be further reduced by reducing the hole size as also presented in Section 3.3 for a perforated plate set in a perforated baffle case.

5.3.2 Radiation by modes of vibration

Eq.(5.5) is now applied for calculating the sound radiation by modes from a simply supported, perforated plate. The point force is excited at one location on the plate.

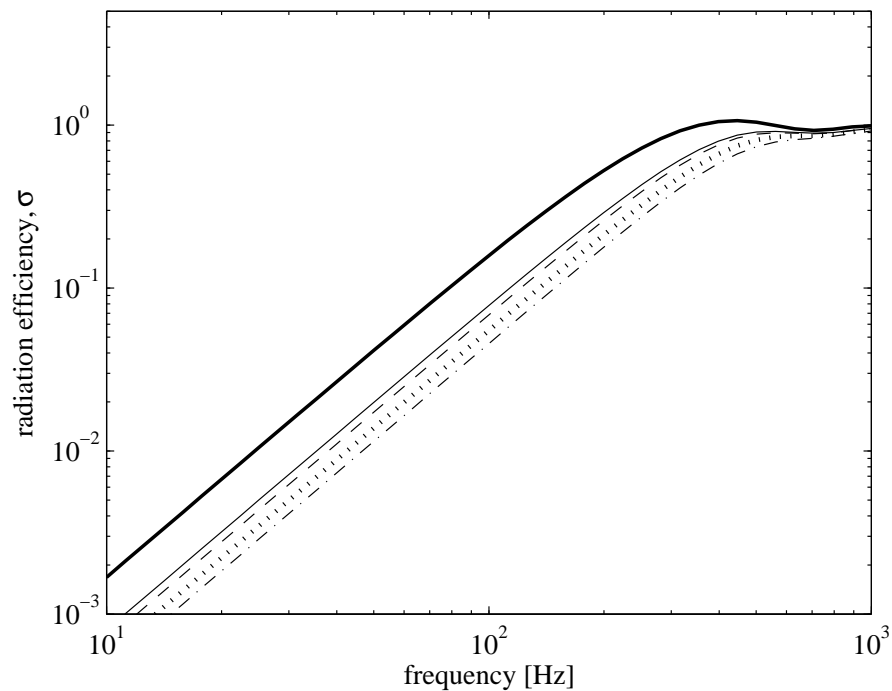


FIGURE 5.4: Radiation efficiency of a perforated baffled plate (rectangular piston) from discrete monopole sources: $0.65 \times 0.5 \times 0.003$ m, $\tau = 4\%$, $dx = 0.02$ m (— unperforated, — $d_o=43$, -- $d_o=33$, \cdots $d_o=26$, $- \cdot -$ $d_o=13$ mm).

For 10×10 modes and the same frequency resolution as the radiation efficiency from a vibrating piston, the calculation time is about 40 s.

Figure 5.5 plots the radiation efficiency for the same plate specifications as in Figure 5.3. The force is applied around the plate corner at $(2dx, 3dy)$ from the origin $(0,0)$. The results show that the radiation efficiency reduces as the perforation ratio increases.

The effect of hole density (number of holes per unit area) on the radiation efficiency is shown in Figure 5.6 where for constant perforation ratio, the sound radiation can again be reduced by increasing the hole density.

The effect of perforation is shown in Figure 5.7. This shows that the sound reduction due to perforation is almost constant below the fundamental mode (70 Hz). The effect of perforation from the baffled piston is also plotted for comparison; these two sets of results diverge a little as the perforation increases. Radiation from modal response shows greater effect of perforation in the fundamental mode and edge mode regions and a lower effect of perforation in the corner mode region than that from the vibrating piston.

Figure 5.8 compares these results with the effect of perforation from an unbaffled perforated plate from Chapter 4. This shows greater differences as the perforation ratio increases particularly at the fundamental edge where the effect of perforation from the perforated baffled plate is greater. Above the fundamental mode region, the perforated

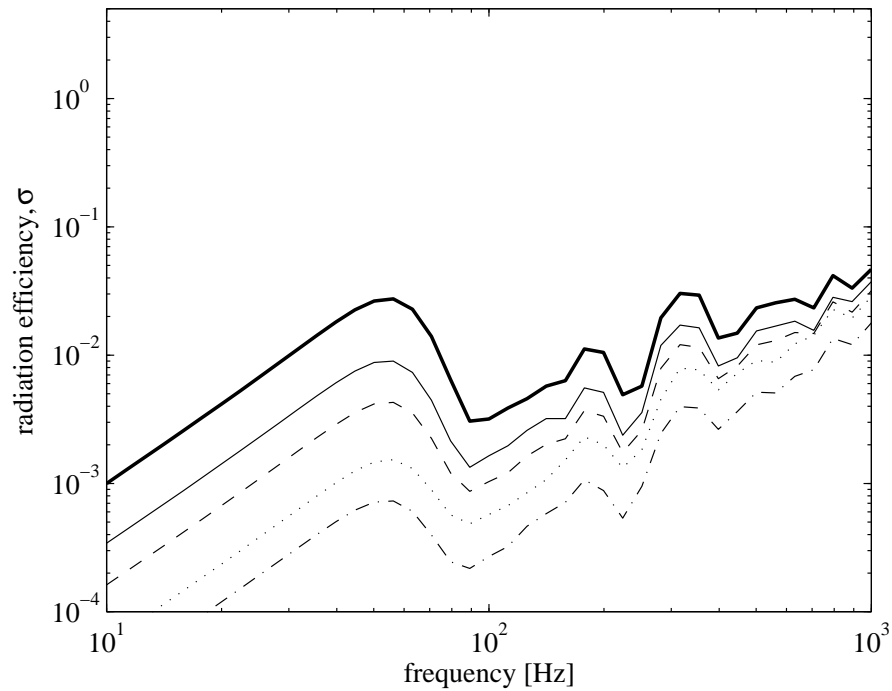


FIGURE 5.5: Radiation efficiency from modal response of a perforated baffled plate from discrete monopole sources: $0.65 \times 0.5 \times 0.003$ m, $d_o = 0.04$ m, $dx = 0.02$ m, $\eta = 0.1$ (— unperforated, - - $\tau=6\%$, - · - $\tau=12\%$, · · · $\tau=22\%$, - - - $\tau=31\%$).

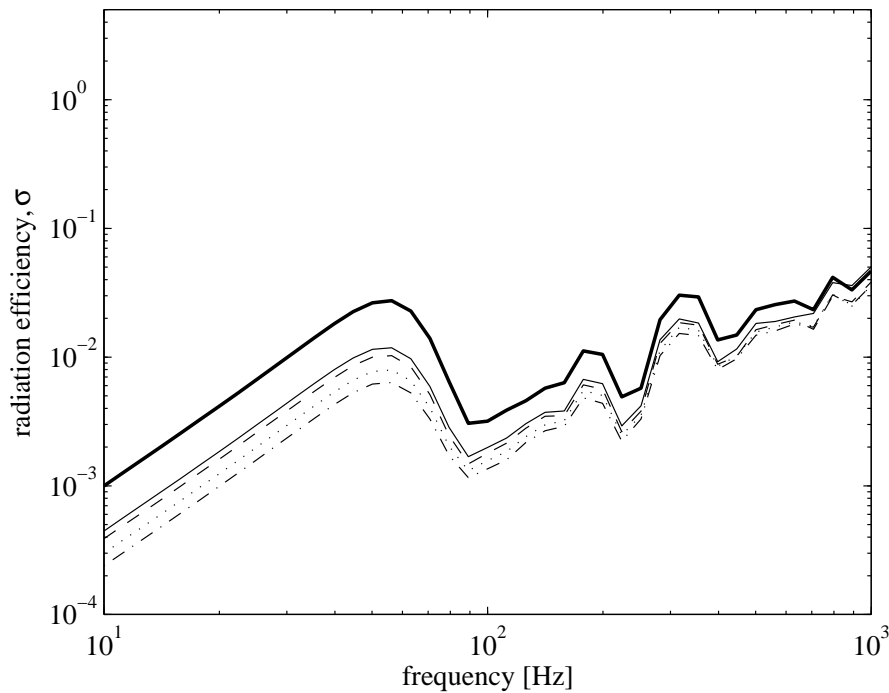


FIGURE 5.6: Radiation efficiency from modal response of a perforated baffled plate from discrete monopole sources: $0.65 \times 0.5 \times 0.003$ m, $\tau = 4\%$, $dx = 0.02$ m (— unperforated, - $d_o=43$, - - $d_o=33$, · · · $d_o=26$, - - - $d_o=13$ mm).

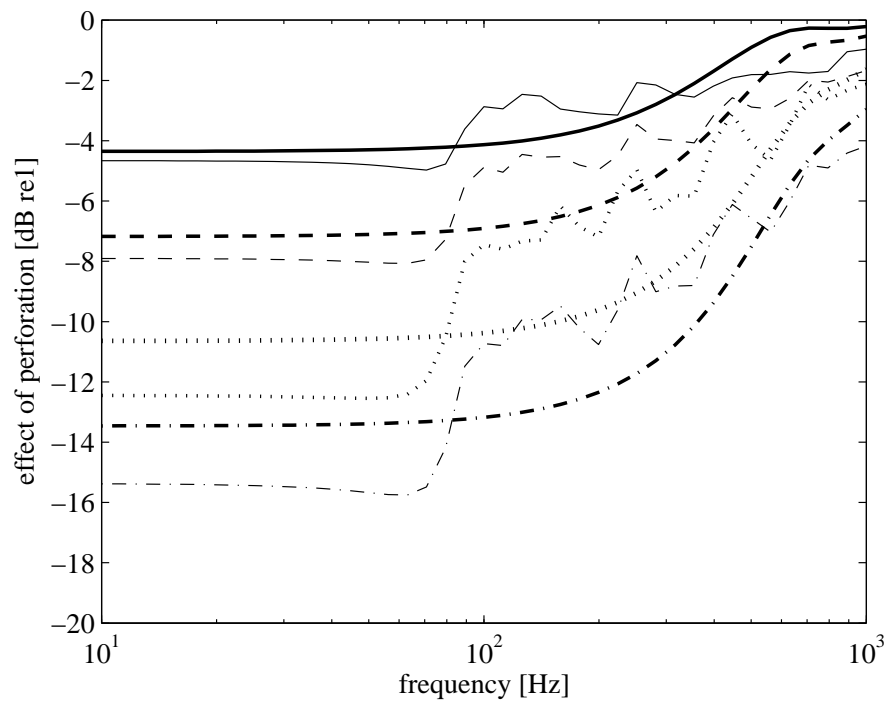


FIGURE 5.7: Comparison of the effect of perforation on sound power radiation of a perforated baffled piston (thick line) with that from the perforated baffled plate of modal response (thin line) from discrete monopole sources: $0.65 \times 0.5 \times 0.03$ m, $d_o = 0.04$ m, $dx = 0.02$ m ($-\tau=6\%$, $--\tau=12\%$, $\cdots\tau=22\%$, $-\cdot-\tau=31\%$).

unbaffled plate gives more reduction of radiated sound. It can be seen that for high perforation ratio the average difference is 4 dB up to 1 kHz.

5.3.3 Frequency limit of continuous impedance

Figure 5.9 presents the the radiation efficiency of perforated plates with a small number of holes in order to have a large hole separation. The hole distances are 0.2 m for 3×3 holes and 0.32 m for 2×2 holes. The unit force is applied at $(12dx, 10dy)$ from the origin $(0, 0)$.

The interesting phenomenon is found around 530 and 850 Hz where the radiation efficiency from the perforated plate exceeds that of the unperforated plate. The phenomenon is more obvious in the effect of perforation, as plotted in Figure 5.10. It can be seen that above f_{l1} for 2×2 holes and f_{l2} for 3×3 holes, the perforated plate does not reduce the radiation (≥ 0 dB). This occurs when the hole distance is at or more than half of the acoustic wavelength. The frequency at this condition is the frequency limit for the assumption of the continuous acoustic impedance.

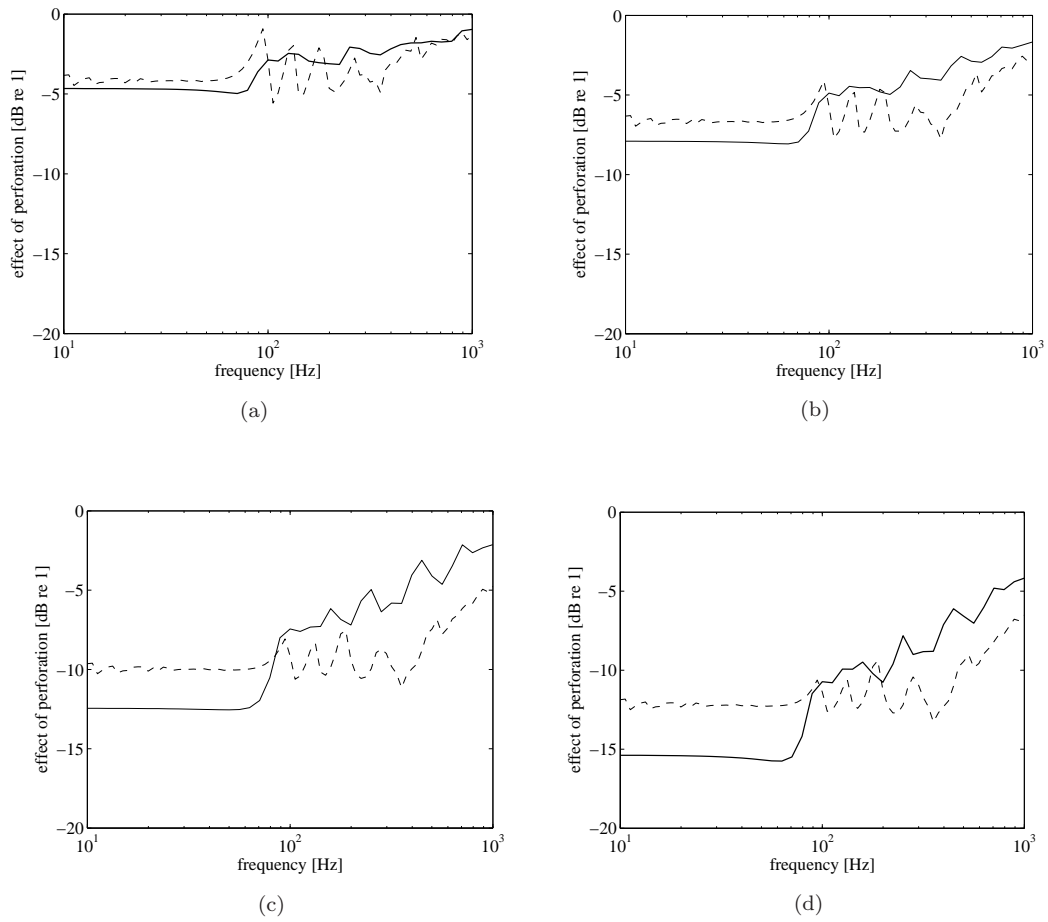


FIGURE 5.8: Comparison of the effect of perforation on sound power radiation of a perforated baffled plate (—) with that of a perforated unbaffled plate (---): $0.65 \times 0.5 \times 0.003$ m, $d_o = 0.04$ m, $dx = 0.02$ m, $\eta = 0.1$; (a) $\tau=6\%$, (b) $\tau=12\%$, (c) $\tau=22\%$, (d) $\tau=31\%$.

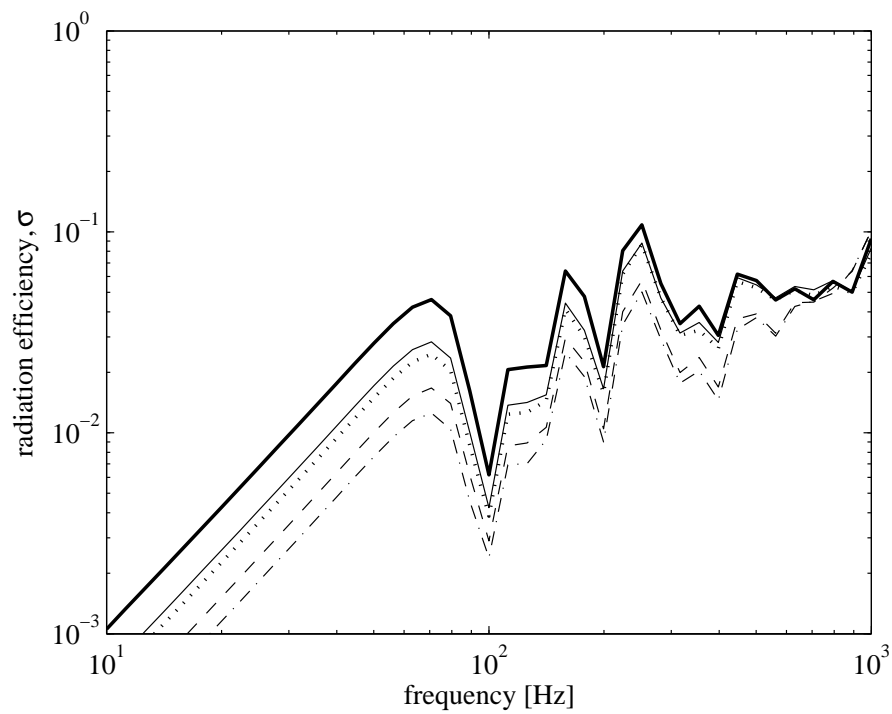


FIGURE 5.9: Radiation efficiency from modal response of a perforated baffled plate from discrete monopole sources showing the frequency limit of continuous impedance assumption: $0.65 \times 0.5 \times 0.003$ m, $dx = 0.02$ m, $\eta = 0.1$ (— unperforated; $d_o = 0.06$ m: — $N_h = 2 \times 2$, — — $N_h = 3 \times 3$; $d_o = 0.075$ m: $\cdots N_h = 2 \times 2$, - · - $N_h = 3 \times 3$).

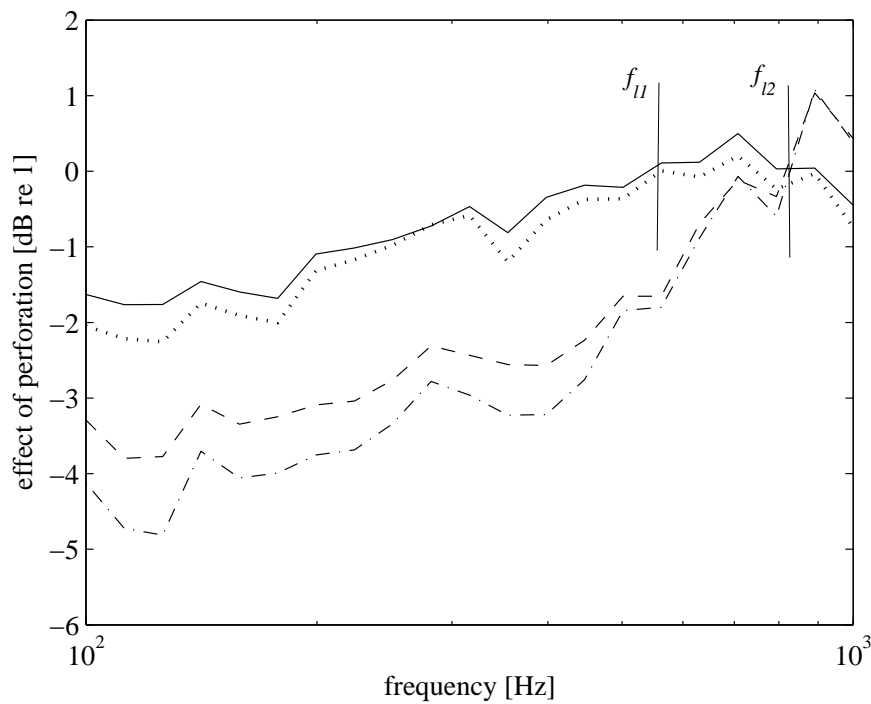


FIGURE 5.10: Effect of perforation from modal response of a perforated baffled plate from discrete monopole sources showing the frequency limit of continuous impedance assumption: $0.65 \times 0.5 \times 0.003$ m, $dx = 0.02$ m, $\eta = 0.1$ ($d_o = 0.06$ m: — $N_h = 2 \times 2$, — — $N_h = 3 \times 3$; $d_o = 0.075$ m: $\cdots N_h = 2 \times 2$, - · - $N_h = 3 \times 3$).

Chapter 6

Conclusions

Several models for calculating the radiation efficiency of perforated plates have been investigated. It is shown that for moderate size of holes (diameters $d_o > 1$ mm), the effect of fluid viscosity in the hole can be ignored. The fluid reaction in the holes is purely inertial. It is also shown that the effect of the near-field from adjacent holes can be neglected even up to high perforation ratios.

The analytical model of a perforated plate set in a perforated baffle can be evaluated considerably more easily than for a rigid baffle or unbaffled plate. Due to the equally perforated baffle, at low frequencies, the radiation efficiency reduces drastically. The plate changes from monopole-like radiator to dipole-like radiator as the perforation is introduced. For this model, the effect of perforation is found to be independent of the plate dimensions.

A model for a perforated unbaffled plate is developed by introducing the perforation parameter into Laulagnet's model. The results shows that the effect of perforation is independent of frequency in the fundamental mode and corner mode regions. At low perforation ratio, the radiation efficiency is smaller than that for the perforated baffle. However, it is found that as the perforation increases, the results of the two models become similar. The effect of the baffle decreases as the perforation ratio increases. Unlike the perforated baffled case, the results show that the effect of perforation depends on both the plate thickness and on the plate dimension. Comparison with existing measured results on an unbaffled perforated plate shows a good agreement except at very low frequencies and high perforation ratio.

Sound radiation from a perforated plate can also be calculated by modelling the plate as discrete monopole sources. This can be done by discretizing the Rayleigh integral. The model provides the sound radiation from a perforated plate set in an infinite rigid baffle. For a vibrating piston, the perforation gives a constant reduction in the radiation

efficiency over the frequency range before it converges to unity. For a vibrating plate with modal response, the constant effect of perforation only occurs in the fundamental mode region. In the corner and edge mode regions, it decreases as the frequency increases. In these regions, the effect of perforation is lower than that of the perforated unbaffled plate.

It is found that when the distance between holes are greater than half the acoustic wavelength, the assumption of a continuous impedance across the plate surface is no longer valid and the perforation no longer reduces the sound radiation.

The results from all the models show that the sound radiation from a perforated plate decreases either as the perforation ratio τ increases or the hole size d_o decreases. In other words, with the same perforation ratio, increasing the hole density (number of holes per unit area of the plate) can reduce the sound radiation.

Appendix A

Sound Radiation by a Uniformly Vibrating Perforated Strip

Fahy and Thompson [7] have developed a model of radiation of a uniformly vibrating perforated strip set in an infinite similarly perforated baffle. This two-dimensional model allows the baffle to have arbitrary specific acoustic impedance. For a strip set in a rigid infinite baffle, the specific acoustic impedance associating with the perforation of the baffle z_{h2} is set to have very large value compared to that associated with the perforation of the plate z_{h1} ($|z_{h1}/z_{h2}| \rightarrow 0$). Meanwhile for an unbaffled perforated strip, the specific acoustic impedance z_{h2} should be very low ($|z_{h1}/z_{h2}| \rightarrow \infty$). The complete mathematical derivation of the method can be found in reference [7].

As mentioned in Introduction, for an unbaffled strip, it is found that the matrix to be inverted is singular or nearly singular, which reduces the quality of the solution. Figure A.1 presents the radiation efficiency of a perforated strip with length L plotted against the non-dimensional parameter kL for the perforated strip set in the similarly perforated baffle ($z_{h2} = z_{h1}$) and in the rigid baffle. For the rigid baffle, the results are proportional to kL at low kL , i.e. it has a frequency dependence of 10 dB/decade. The perforation of the baffle drastically changes the frequency dependence of the radiation efficiency to 30 dB/decade. The results are proportional to $(kL)^3$ and the radiation efficiency for the perforated baffled is lower than that for the rigid baffle. Figure A.2 shows the radiation efficiency of the unbaffled perforated strip compared with that of the perforated strip set in the rigid baffle. The results for the unbaffled perforated strip are expected to be lower than those for the rigid baffle but have the same frequency dependence at low kL . As seen in the figure, the inverted near-singular matrix gives poor quality results.

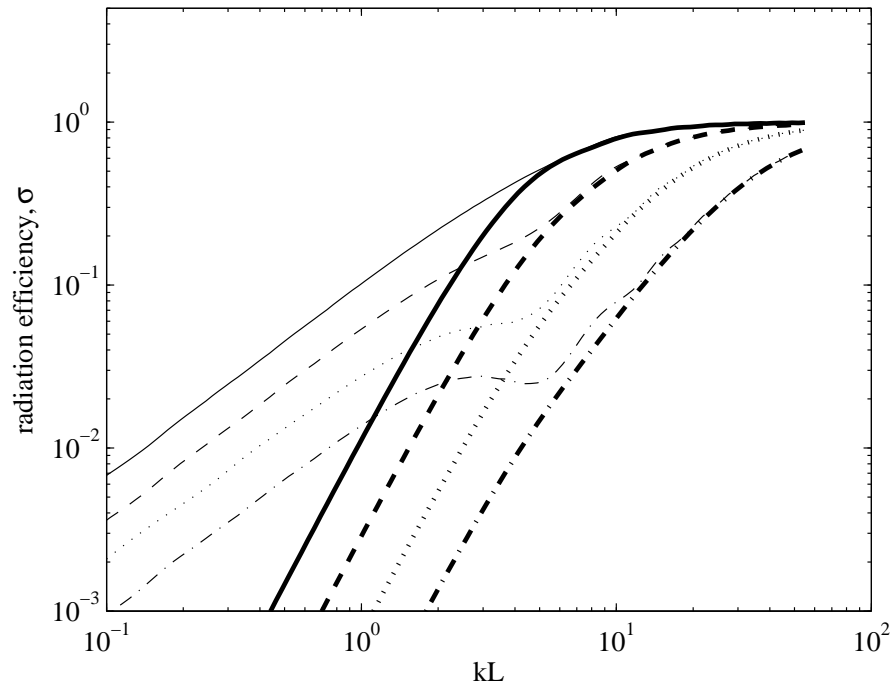


FIGURE A.1: Radiation efficiency of a strip-piston in a perforated baffle (thick line) and in a rigid baffle (thin line): $-h/kL=0.44$, $--h/kL=0.22$, $\cdots h/kL=0.11$, $- \cdot -h/kL=0.055$.

Both results from Figure A.1 and Figure A.2 are presented for different h/kL where h is the non-dimensional specific acoustic impedance as defined in Section 5.1.4. The strip itself has implicitly an infinite width. Consequently, arbitrary number of holes can be introduced even though they are limited in the strip length direction. Therefore it is convenient to represent a non-dimensional parameter as a function of the surface area of the strip (plate), the area of the hole and the perforation ratio.

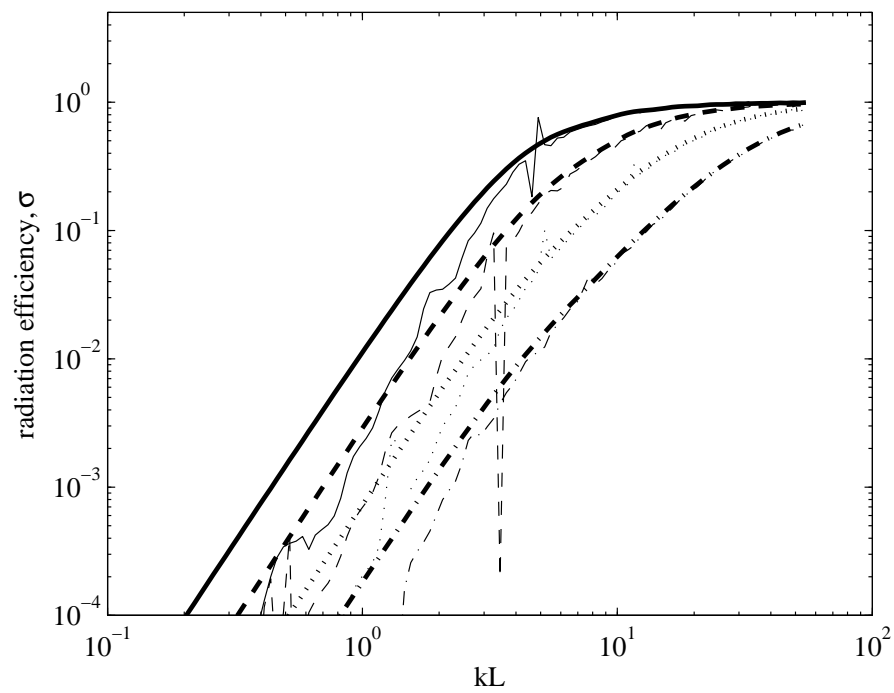


FIGURE A.2: Radiation efficiency of a strip-piston in a perforated baffle (thick line) and in a low impedance baffle ($z_{h1} = 0.1z_{h2}$, thin line): $-h/kL=0.44$, $--h/kL=0.22$, $\cdots h/kL=0.11$, $- \cdot -h/kL=0.055$.

References

- [1] D. Takahashi and M. Tanaka. Flexural vibration of perforated plates and porous elastic materials under acoustic loading. *Journal of the Acoustical Society of America*, 112(4):1456–1464, 2002.
- [2] Y. Y. Lee, E. W. M. Lee, and C. F. Ng. Sound absorption of a finite flexible micro-perforated panel backed by an air cavity. *Journal of Sound and Vibration*, 287:227–243, 2005.
- [3] M. Toyoda and D. Takahashi. Reduction of acoustic radiation by impedance control with a perforated absorber system. *Journal of Sound and Vibration*, 286:601–614, 2005.
- [4] M. Toyoda, M. Tanaka, and D. Takahashi. Reduction of acoustic radiation by perforated board and honeycomb layer systems. *Applied Acoustics*, 68:71–85, 2007.
- [5] M. H. A. Janssens and W. J. van Vliet. Noise from steel bridges: research into the effect of perforations of bridge components (in dutch). Technical report, TNO report TPD-HAG-RPT-960057, 1996.
- [6] D. Y. Maa. Microperforated panel wideband absorber. *Noise Control Engineering Journal*, pages 77–84, November-December 1987.
- [7] F. J. Fahy and D. J. Thompson. The effect of perforation on the radiation efficiency of vibrating plates. *Proceedings of the Institute of Acoustics*, 26, 2004.
- [8] B. Laulagnet. Sound radiation by a simply supported un baffled plate. *Journal of the Acoustical Society of America*, 103(5):2451–2462, 1998.
- [9] L. Rayleigh. *The Theory of Sound*. 2nd edition, 1896.
- [10] I. B. Crandall. *Theory of Vibration System and Sound*. Van Nostrand, New York, 1926.
- [11] P. M. Morse and U. Ingard. *Theoretical Acoustics*. McGraw-Hill, New York, 1968.

-
- [12] F. J. Fahy. *Sound and Structural Vibration: Transmission and Response*. Academic Press, London, 1985.
- [13] D. Y. Maa. Potential of microperforated panel absorber. *Journal of the Acoustical Society of America*, 104(4):2861–2866, 1998.
- [14] A. D. Pierce. *Acoustics*. Acoustical Society of America, 1989.
- [15] L. V. King. On the electrical and acoustic conductivities of cylindrical tubes bounded by infinite flanges. *Philosophical Magazine*, 21(7):128–144, 1936.
- [16] L. E. Kinsler, A. R. Frey, A. B. Coppens, and J. V. Sanders. *Fundamentals of Acoustics*. John Wiley and Sons, 3rd edition, 1982.
- [17] G. Xie, D. J. Thompson, and C. J. C. Jones. The radiation efficiency of baffled plates and strips. *Journal of Sound and Vibration*, 280:181–209, 2005.
- [18] A. Putra and D. J. Thompson. Sound radiation from plates with mixed impedance boundary conditions. Technical report, ISVR Technical Memorandum 957, University of Southampton, 2005.
- [19] R. A. Pierri. Study of a dynamic absorber for reducing the vibration and noise radiation of plate-like structures. Master’s thesis, Institute of Sound and Vibration Research, University of Southampton, 1977.
- [20] A. Putra and D. J. Thompson. The radiation efficiency of point-excited rectangular baffled and unbaffled plates. *Proceedings of the Institute of Acoustics*, 28(1), 2006.
- [21] L. Cremer, M. Heckl, and B. A. T. Petersson. *Structure-borne sound*. Springer, Berlin, 3rd edition, 2005.